



# Effects of soil small strain nonlinearity on the dynamic behavior of floating column structures considering soil-structure interaction

Palani Jagan<sup>1</sup> · Joseph Antony Visuvasam<sup>1</sup>

Received: 8 January 2024 / Accepted: 30 April 2024 / Published online: 29 May 2024  
© Springer Nature Switzerland AG 2024

## Abstract

Past seismic events reveal that soil and structural responses are interdependent, not independent. The seismic behavior of irregular structures, considering soil-structure interaction (SSI) effects, significantly increases the structural vulnerability compared to traditional fixed-base structures. The study on the impact of SSI on irregular structures, especially those with floating columns, is currently limited. Hence, this study primarily examines the influence of nonlinear soil structure interactions on the dynamic response of mid-rise reinforced floating column structures resting on different soil mediums. A three-dimensional finite element programming tool is used to simulate the seismic response of structures with and without floating columns. This study explores the use of elastoplastic hinges to study the inelastic behavior of structural components. The isotropic hardening elastoplastic hysteretic soil model is used to account for the nonlinear behavior of the soil. The nonlinear time history analysis is used to perform and evaluate structural demand parameters subjected to selected ground motions. Moreover, the seismic structural response parameters, such as storey displacement, peak storey drift, peak horizontal acceleration, base shear, and member forces, are compared for both fixed and SSI bases. The analysis results show that the presence of floating columns in structures significantly alters the dynamic response of buildings compared to those without floating column structures. The incorporation of SSI effects increases the flexibility of the foundation and increases the seismic structural response of storey displacement and inter-storey drift ratio while reducing the base shear value.

**Keywords** Floating column · Soil structure interaction · HSS constitutive model · PLAXIS 3D · Nonlinear time history analysis · Inter storey drift

## Introduction

Soil-structure interaction (SSI) is a phenomenon in which the response of the soil affects the motion of the structure, and the response of the structure affects the motion of the soil [1]. Due to seismic events, the interaction between soil response and structural response demonstrates that their responses are interdependent rather than independent. However, the standards for structural design recommended either ignoring the effects of SSI or concession a reduction in the seismic coefficient when accounting for SSI effects. Seismic design guidelines for SSI [2, 3] show that consensus and

recommend reducing base shear when SSI has to be taken into account. According to IS: 1893 (Part 1-2002) [4], it is not recommended to incorporate soil-structure interaction (SSI) in the seismic design of structures built on rock-type materials. Moreover, the presence of tall buildings on soft soil can significantly alter the seismic response of the structure due to SSI effects during an earthquake event [5].

Several researchers [6–8] have examined seismic structural behavior incorporation of SSI effects due to earthquakes. SSI has significantly affected dynamic structural responses and it is crucial to consider this during the design process. Also, the dynamic responses of multi-story reinforced concrete frame buildings resting on raft foundations, considering SSI effects, have been investigated [9–11]. These studies have revealed that factors such as the number of stories, soil type, soil damping, stiffness degradation, distinctive foundation behaviors, and ground motion characteristics play a significant role in influencing seismic structural behavior. Many researchers [12–15] have performed

✉ Joseph Antony Visuvasam  
visuvasam.j@vit.ac.in

Palani Jagan  
jagan.p2020@vitstudent.ac.in

<sup>1</sup> School of Civil Engineering, Vellore Institute of Technology, Vellore, Tamil Nadu 632014, India

the nonlinear dynamics analysis by using finite element programming tools to evaluate the seismic structural response. The findings of these studies concluded that the stiffness of the soil, and frequency content of the ground motions are the most important factors affecting SSI. Also, if the rigidity of the soil is reduced, structural floor-level displacement increases.

Due to global urbanization, irregular structures are becoming more widespread. The shapes and orientations of structures are modified due to functional, aesthetic, and usage requirements. Several codes [4, 16–18] provided recommendations and guidelines for earthquake-resistant design of irregular structures, and it is periodically revised due to increased demand and emerging difficulties. Vertical irregularity relates to the varying structural characteristics over the height of structures. This variation incorporates changes in the geometrical shape, mass distribution, strength, and stiffness along the structural height. In the past seismic events, such as the earthquakes in Mexico (2017), Kobe (1995), and Northridge (1994), have demonstrated the adverse effects of vertical irregularities in structures when subjected to seismic forces. Several researchers [19–21] have performed static and dynamic inelastic analyses to evaluate the seismic response of vertical irregular structures. Ghoozhi et al. [22] studied the seismic behavior of tall ground-storied structures with irregular configurations, considering the effects of SSI. They concluded that accounting for SSI is crucial for reducing seismic demand, especially in soft soil conditions.

The column is supported by a beam or transfer slab and not directly attached to the foundation is called a floating column. The presence of discontinuities in column elements leads to a deficiency in load transmission paths during lateral forces, resulting in poor performance of structures. Various researchers [23–26] conducted a comparative analysis of the seismic performance of structures with and without floating structures. The results showed that floating column structures modify the spectral acceleration and base shear, extend the time period, and increase storey displacement. Singala and Rahaman [24] conducted static and dynamic analyses on a structure with floating columns, as depicted in Fig. 1. This evaluation aimed to assess the seismic effects of floating column structures in multistoried RC buildings. The study concluded that the presence of floating column structures significantly alters the dynamic response of buildings. Additionally, lower-level stories of structures experienced increased vulnerability to earthquake forces. Several authors [27–30] reported that floating column structures and the variation in lateral stiffness on each floor of the building greatly influence the structural vulnerability during earthquakes. Consequently, this leads to increased structural lateral displacement. Jagan and Visuvasam [31] performed an analysis of the inelastic seismic behaviors of reinforced

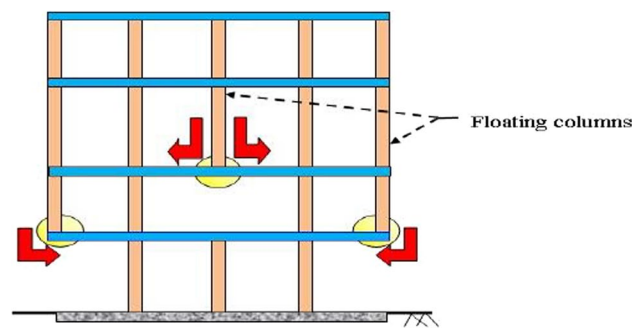


Fig. 1 Structure with floating columns

concrete buildings with and without floating columns. The study results reveal that the presence of floating columns increases the inter-storey drift ratio and structure damage probability. Bhosle et al. [32] have investigated the seismic response of vertical irregular structures. The findings show that structures with open-ground stories and floating column structures demonstrate increased vulnerability in comparison to regular structures. However, urban development has led to the construction of these irregular structures, which are difficult to control. Modern construction techniques enable the creation of flexible structures with unique shapes and aesthetics. At the same time challenge traditional principles and raise safety concerns due to their unconventional design.

From the previous literature studies, floating column structures are more vulnerable to earthquake forces compared to conventional structures. Therefore, suitable retrofitting methods are required to minimize the structural vulnerability of floating column structures in seismic-prone areas. Several researchers [33–36] have studied different retrofitting techniques to mitigate the seismic vulnerability of floating column structures. For example, lateral load-resisting systems such as moment-resisting frames, shear wall structures, and structures with various bracing systems (including diagonal, X, K, V, and inverted V) are widely used retrofitting techniques in floating column structures. Saeed et al. [37] conducted a recent numerical study on the seismic performance of shear walls in buildings with regular and staggered openings. The dynamic analysis was performed to assess the seismic response parameters and compare the performance of shear walls with regular and staggered openings in buildings. The authors concluded that openings have a significant effect on the seismic behavior of shear walls, emphasizing the necessity of considering them during the construction design phase. Additionally, various authors [38, 39] have focused on enhancing the mechanical strength and shear performance of reinforced concrete beams. The findings of the studies contribute to the development of stronger building materials and structural elements, enhancing seismic resistance.

Based on the literature studies, it is indicated that seismic responses of irregular structures considering SSI effects are more susceptible. Previous studies have mainly focused on the seismic behavior of structures with floating columns, neglecting the impact of SSI effects. However, there is limited research on the inelastic seismic response of floating columns considering nonlinear dynamic soil-structure interaction. Hence, further investigations are necessary to understand the comprehension of the vulnerability of floating column structures considering SSI effects. This study aims to provide valuable insights into the response of reinforced concrete floating column structures under seismic loading, considering nonlinear dynamic soil-structure interactions. The five-storied structures rest on a raft foundation embedded in different soil mediums. Nonlinear time history analysis (NLTHA) is performed to assess the structural responses for both fixed and SSI (flexible) bases. The present study involves, finding the seismic structural response parameters such as peak lateral storey displacement, peak storey drift, peak horizontal acceleration, base shear, and member forces. The numerical results aid in comparing the structural response characteristics of various soil strata in a moderate seismic zone.

### Description of structure properties

The five-storied reinforced moment-resistant concrete frame structures are used in this numerical study. The ground floor height is 4.5 m and the remaining floor height is 3.5 m. The total height of the building is 18.5 m. The plan dimensions of the structure at ground floor level are 16 m × 15 m. The structure comprises four bays in the longitudinal direction, each with equal intervals of 4 m, and three bays in the lateral direction, with intervals of 5 m. This study involves four different types of structural models. One of the models represents a regular structure without floating columns (Fig. 2a), while the other three models incorporate floating columns oriented in different directions such as X (Fig. 2b), Y (Fig. 2c), and XY (Fig. 2d). In addition to the regular structures, a 1.5 m bay width is extended from the outer columns of the structure at the first-floor level. The floating columns are positioned at the end of these extended bays. Furthermore, the floating columns begin at the first-floor level and extend up to the roof level. These types of floating columns are not supported by the ground. The dimensions of the structural elements are provided in Table 1. A uniform slab thickness of 15 cm was utilized for all models. The used concrete properties are compressive strength ( $f_{ck}$ ), unit weight ( $\gamma$ ) and the Poisson ratio are 30 N/mm<sup>2</sup>, 25 kN/m<sup>3</sup>, and 0.2 respectively [40].

The value of modulus elasticity is 27386 MPa, calculated using the relationship of  $5000\sqrt{f_{ck}}$  as per IS 456-2000 [40].

The yield strength of steel ( $f_y$ ) is 500 N/mm<sup>2</sup>. According to IS 875 [41] the gravity loads are taken into account. The dead load is considered as the self-weight of structural elements and addition floor finish (1.0 kN/m<sup>2</sup>) and live load (3.0 kN/m<sup>2</sup>).

The structural ductility in a moment-resisting frame relies on the bending capacity of beams. Components with ductile behavior can undergo plastic deformation without a significant reduction in strength. Consequently, these components absorb and dissipate the energy from seismic forces. Thus, the elastoplastic hinge element (nonlinear flexure/bending spring) was utilized at beam ends to simulate the nonlinear behavior of the building [42, 43]. The bending stiffness ( $EI$ ) at the end of the beam, and the plastic moment ( $M_n = M_p$ ) are defined as follows

$$E_c I_{eff} = 0.35 E_c I_g \text{ for beams} \tag{1}$$

$$M_n = M_p = A \sigma_y y_g$$

$$E_c I_{eff} = M_n / 2 \epsilon_y \text{ for columns} \tag{2}$$

where,  $E_c$  = concrete elastic modulus,  $I_g$  = gross moment of inertia,  $A$  = sectional area,  $y_g$  = distance between centroid of tensioned or concrete zones of cross section and neutral axis,  $\epsilon_y$  = yield strain of steel reinforcement,  $\sigma_y$  = compressive strength of concrete (assumed to equal to compressive strength of concrete,  $f'_c$ ). The cracking effects are taken into consideration by assuming the cracked column and beam were 0.7 and 0.35 times the bending stiffness of uncracked components, respectively. It is assumed that the structural models are located in Chennai. Based on the guidelines provided by IS 1893-2016 [44] the Chennai site location falls within Zone III and is categorized as a moderate seismic zone. The seismic design characteristics of the site include the zone factor (Z), response reduction factor, importance factor, and damping, which are adapted to be 0.16, 5, 1.5, and 5%, respectively. The analysis and design of super-structural elements using structural analysis programming (SAP 2000) [45]. The structures are analyzed by using both equivalent static and response spectrum analyses. As per IS 456-2000 [40] the permissible storey drift due to lateral forces is 0.4% of the storey height. The analysis results for all models ensured that the lateral storey drift values were within the permissible limits.

### Finite element modelling of the soil-raft-structure system

The finite element programming tool is utilized to simulate the interaction between the soil and structure in the direct analysis approach. This study examined the seismic response

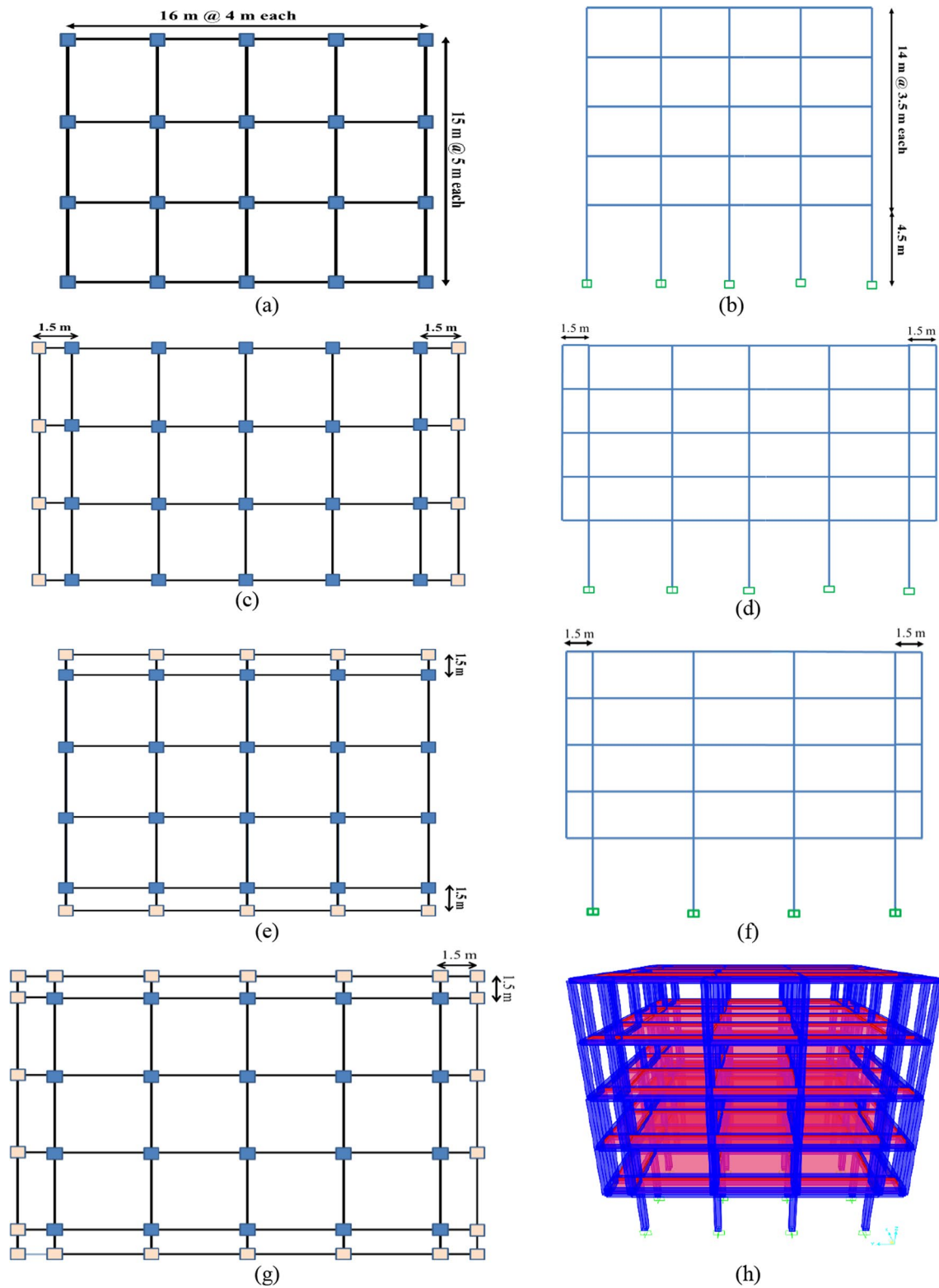


**Fig. 2** Typical plan and sectional elevations of structures. **a** Ground floor plan for without floating column structure, **b** sectional elevation view for without floating column, **c** first-floor plan view for floating in X direction, **d** sectional elevation view for floating in X direction,

**e** first-floor plan view for floating in Y direction, **f** sectional elevation view for floating in Y direction, **g** first-floor plan view for floating in XY direction, **h** three-dimensional view of floating XY structures

**Table 1** Dimension of structural elements for all models

Structure type	Floor level	Beam size (m)		Column size (m)
		Inner and Peripheral columns	Cantilever beams starting from the first-floor level	
Without floating column (WOF)	Ground floor	0.30×0.45	–	0.40×0.55
	1st and 2nd floor	0.30×0.40	–	0.40×0.50
	3rd and 4th floor	0.25×0.30	–	0.35×0.45
Floating column in the X direction (FX)	Ground floor	0.30×0.45	0.35×0.65	0.45×0.55
	1st and 2nd floor	0.30×0.45	0.35×0.45	0.40×0.50
	3rd and 4th floor	0.25×0.30	0.25×0.30	0.35×0.45
Floating column in the Y direction (FY)	Ground floor	0.35×0.50	0.35×0.70	0.45×0.60
	1st and 2nd floor	0.35×0.45	0.35×0.45	0.40×0.55
	3rd and 4th floor	0.25×0.30	0.25×0.30	0.35×0.50
Floating column in XY direction (FXY)	Ground floor	0.35×0.50	0.35×0.75	0.45×0.60
	1st and 2nd floor	0.35×0.45	0.35×0.45	0.40×0.50
	3rd and 4th floor	0.25×0.30	0.25×0.30	0.25×0.30

of five-story reinforced concrete structures with and without floating columns resting on raft foundations supported by different soil mediums. The foundation is embedded at a depth of 1.5 meters below ground level. A raft foundation with a thickness of 450 mm and a plan dimension of 19 m by 18 m has been adopted. The model depicts a beam and column with six-node beam elements made of linear elastoplastic materials. Additionally, slab and raft components are represented by 6-noded plate elements with linear elastic properties, whereas soil elements are represented by 10-noded tetrahedral elements. Previous studies [46, 47] suggested that the geometric soil model boundaries are seven times raft width to minimize boundary effects and wave reflection. The schematic diagram in Fig. 3 depicts the soil-foundation-structure system without floating column models and a similar approach used for floating column structures. The hardening soil with small strain (HSS) constitutive model is used to simulate the nonlinear dynamic behavior of structures during earthquakes.

**Soil properties**

The majority of soil standards classify the state of the soil condition according to shear wave velocity. This study aims to examine three different soil types, as classified according to the International Building Code (IBC) [48]. The basic properties of different soil mediums utilized in this study such as hard, stiff, and soft are presented in Table 2. This study assumes subsoil homogeneity and constant shear wave velocity throughout depth. The water table is assumed much below ground level. The well-defined empirical correlation proposed by Maheswari et al. [49] for all soil conditions in the Chennai zone, as depicted in Eq. 3, is employed in this study to determine the SPT-N value for various soil

mediums. Additionally, the structural models utilized in this study are assumed to be located in Chennai. Therefore, this correlation is very helpful in deriving the soil properties for different soil mediums in this present study. It is important to note that the SPT-N values were determined using this correlation in Eq. 3 for various soil conditions in this study fall within the range of Indian soil types specified in IS 1893-2016 [44], as listed in Table 2. According to Bowels [50], the bulk density ( $\rho$ ) of different soil mediums concerning SPT (N) value was considered for this study. Additionally, the initial shear modulus was determined using linear elasticity, as shown in Eq. 4. The plastic parameter angle of friction in various soil types is taken from Peck et al. [51].

$$V_s = 95.64N^{0.420} (r^2 = 0.84) \text{ [All type soil]} \tag{3}$$

$$G_o = \rho \cdot (V_s)^2 \tag{4}$$

where,  $V_s$  is the shear wave velocity of soil,  $N$  is standard penetration number, and ( $G_o$ ) is initial shear modulus.

**Hardening soil model with small strain stiffness (HSS) model**

The nonlinearity of soil behaviors is essential to understanding the ground response during an earthquake. In this study, the nonlinear analysis of the soil structure system is carried out using the hardening soil model with a small strain stiffness (HSS) constitutive model. To simulate the nonlinear behaviors of soil, the hardening soil (HS) model is one of the advanced constitutive models, which is derived based on the theory of plasticity [52]. The HSS model is an extended version of the hardening soil model

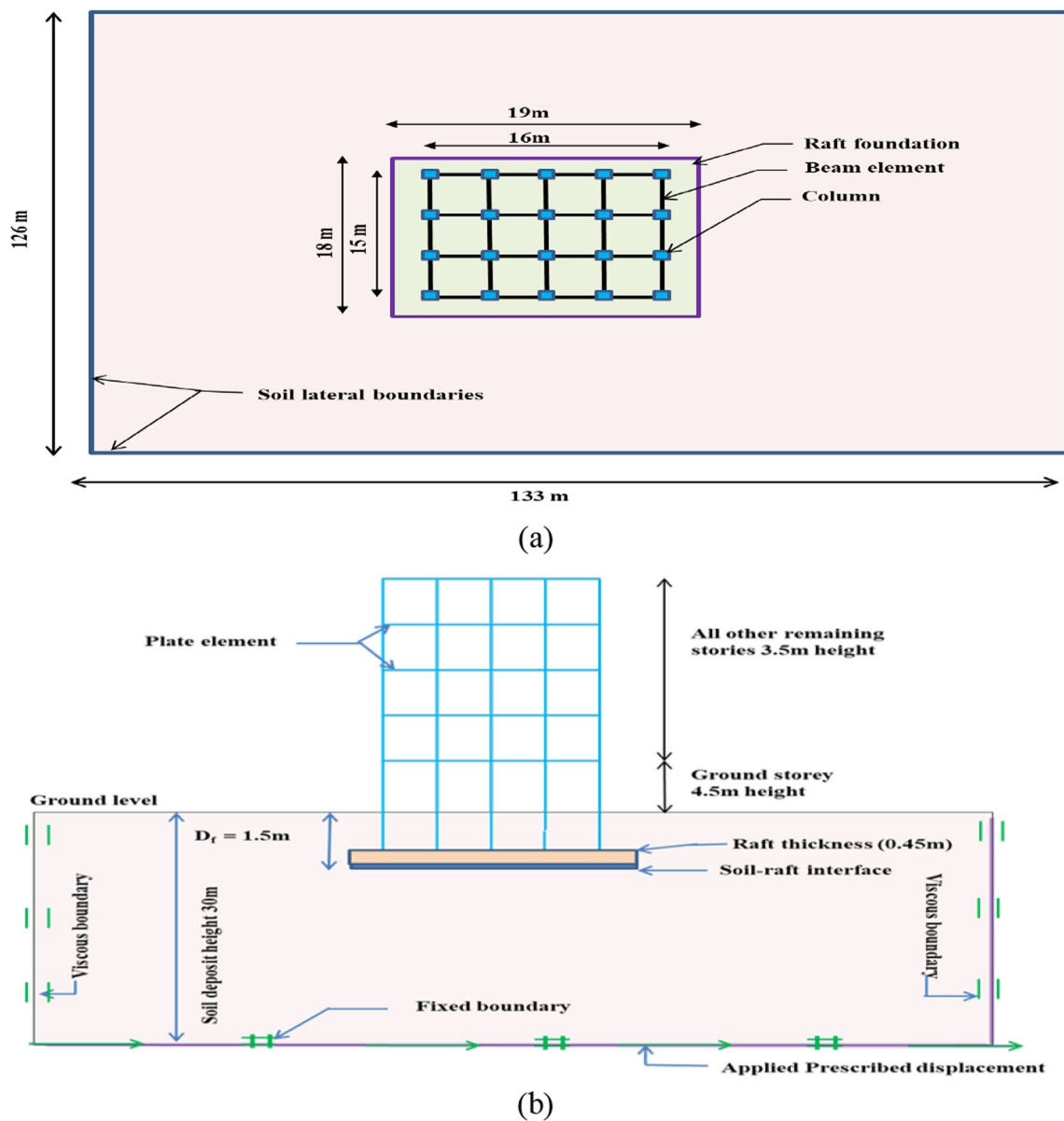


Fig. 3 Modeling of the soil-raft-structure system (without floating column structure). a plan and b sectional elevation

Table 2 Properties of different soil mediums

Soil type	Soil profile as per (IBC)	Shear wave velocity, ( $V_s$ )(m/s)	Average shear wave velocity, ( $V_s$ )(m/s)	Standard penetration number ( $N$ )	Soil type (According to IS 1893–2016 based on SPT- $N$ value)
C	Hard soil	$360 < V_s < 750$	564	$> 50$	$N > 30$ (Hard soil)
D	Stiff soil	$180 < V_s < 360$	260	28	$10 < N < 30$ (Stiff soil)
E	Soft soil	$V_s < 180$	160	6	$10 < N$ (Soft soil)

and has almost similar properties to the hardening soil model. In addition, two additional parameters were added to the HSS model, namely the small-strain shear modulus

( $G_0$ ) and the shear strain level  $\gamma_{0.7}$ , at which the secant shear modulus ( $G_s$ ) is 70% of  $G_0$  [53]. The HSS model accurately accounts for small strain stiffness and nonlinear

strain dependence. This characteristic represents a strength of the HSS model in comparison to other models [54]. The derivation of the variation in the reduced shear modulus curve is shown in Eq. 5, can be achieved by utilizing the hyperbolic law, which was originally proposed by Hardin and Drnevich [55] in Eq. 5.

$$\frac{G_s}{G_0} = \frac{1}{1 + 0.385 \frac{\gamma}{\gamma_{0.7}}} \tag{5}$$

The relationship between shear modulus reduction and strain leads to the determination of the tangent shear modulus ( $G_t$ ), which is constrained by a lower limit at high levels of strain.

$$G_t = \frac{1}{\left(1 + 0.385 \frac{\gamma}{\gamma_{0.7}}\right)^2} \tag{6}$$

The lower cut-off of  $G_t$  is called the unloading–reloading shear modulus ( $G_{ur}$ ), which can be correlated with the unloading–reloading elastic modulus ( $E_{ur}$ ) and Poisson's ratio ( $\nu$ ).

$$G_t \geq G_{ur} = \frac{E_{ur}}{2(1 + \nu_{ur})} \tag{7}$$

The shear modulus, a stress dependency parameter, increases with soil depth and it can be determined by the Eq. 8 [53].

$$G_0 = G_0^{ref} \left( \frac{c' \cos \varphi' - \sigma'_3 \sin \varphi'}{c' \cos \varphi' + p^{ref} \sin \varphi'} \right)^m \tag{8}$$

Based on Eq. 8, the initial shear modulus at a certain stress level or depth is a function of strength parameter  $C$  and  $\varphi$  at the reference pressure of 100 kPa, confining pressure  $\sigma_3$  and power for stress-level dependency ( $m$ ). Equation 8 shows the stress dependence of the shear modulus, which is similar to the stress dependency observed in Young's modulus during unloading and reloading stress paths ( $E_{ur}$ ), the secant modulus ( $E_{50}$ ), and the tangent modulus ( $E_{oed}$ ). The parameter  $E_{50}$  represents the stiffness modulus for primary loading, which is dependent on the confining stress. It can be calculated using the following Eq. 9.

$$E_{50} = E_{50}^{ref} \left( \frac{c' \cos \varphi' - \sigma'_3 \sin \varphi'}{c' \cos \varphi' + p^{ref} \sin \varphi'} \right)^m \tag{9}$$

The  $E_{50}$  value of the soil was calculated in this study by using the SPT- $N$  values and shear strength parameters by the established correlations (Eqs. 10 and 11) for coarse-grained soil (GW-Well graded gravel and S-normal consolidated sand) [50].

$$E_{50} = 1200(N + 6) \text{ for GW} \tag{10}$$

$$E_{50} = 500(N + 15) \text{ for S} \tag{11}$$

According to previous literature studies [56, 57] in the absence of laboratory data, the following relationship ( $E_{50}^{ref} = E_{oed}^{ref} = 3E_{ur}^{ref}$ ) is used to determine the soil stiffness values of  $E_{ur}^{ref}$  and  $E_{oed}^{ref}$ . The soil properties and HSS model parameters utilized in this study are described in Table 3.

The dynamic properties of soil, including the damping ratio and shear modulus, are significant factors for assessing ground response during an earthquake [57]. Therefore, it is essential to consider the nonlinear characteristics of soil during the evaluation of structural seismic response. To enhance the accuracy of predicting the response of soil-foundation-structure systems, the authors Amorosi et al. [58] recommended the utilization of viscous damping in finite element analysis and the incorporation of the Rayleigh formulation. In this approach, the formation of the damping matrix involves combining the mass and stiffness matrices by the linear relationship described in Eq. 12.

$$[C] = \alpha_R [M] + \beta_R [K] \tag{12}$$

The damping, mass, and stiffness matrices are represented by  $[C]$ ,  $[M]$ , and  $[K]$ , respectively. Additionally, the damping coefficients are denoted as  $\alpha_R$  and  $\beta_R$ . The damping coefficients are determined by evaluating the damping ratio associated with two distinct vibration modes occurring at their respective natural frequencies shown in Eq. 13.

$$\begin{pmatrix} \alpha_R \\ \beta_R \end{pmatrix} = \frac{2\xi}{\omega_i + \omega_j} \begin{bmatrix} \omega_i \omega_j \\ 1 \end{bmatrix} \tag{13}$$

where  $\omega_i$  and  $\omega_j$  are two natural modes and their respective frequencies.  $\xi$  assumed damping value for the natural mode. The structural seismic response is most significantly

**Table 3** Soil properties and HSS model parameters used in the analysis

Soil type	$\gamma$ (kN/m <sup>3</sup> )	$c$ (kPa)	$\varphi'$	$E_{50}^{ref}$ (MPa)	$E_{oed}^{ref}$ (MPa)	$E_{ur}^{ref}$ (MPa)	$G_{o,ref}$ (MPa)	$\gamma_{0.7}$ (%)	$\nu_{ur}$	$m$
Hard soil (Soft rock)	21	0	39	127.2	127.2	381.6	713.4	0.0079	0.2	0.5
Stiff soil (Dense sand)	18	0	36	21.5	21.5	64.5	130.1	0.0162	0.2	0.5
Soft soil (Loose sand)	15	0	30	10.5	10.5	31.5	39.1	0.0164	0.2	0.5

affected by the first two vibration modes [59, 60]. Kramer [1] provided the following equation for determining the natural frequencies of soil deposits.

$$f_n = \frac{V_s}{4H}(2n - 1) \tag{14}$$

where,  $f_n$  = natural frequency of the corresponding mode,  $V_s$  = sheare wave velocity,  $H$  = depth of soil deposit, and  $n$  = mode number. Here, the first and second vibration modes of soil deposits with a specific target damping ratio of 5% were selected. The determined damping coefficients are presented in Table 4, where the corresponding values remain constant with depths.

The present study incorporates the consideration of a nonlinear soil model to accurately characterize the dynamic behavior of soil during analysis. The rate at which cyclic shear strain increases has the effect of reducing the tangent shear modulus and increasing the damping ratio during an earthquake. Hence, the consideration of strain, shear modulus, and damping relationships is crucial. The backbone curve is utilized to represent the hysteresis damping. Furthermore, the DEEPSOIL [61] program was utilized to obtain fitting curves, considering the relevant soil parameters that were chosen in this study. The recommended curvature of the backbone for sand layers, as proposed by Seed and Idriss (Mean) [62] is shown in Fig. 4 (as an example of soft soil).

**Table 4** Raylieghs damping coefficients

Soil Type	Natural frequency (rad/s)		Damping coefficients	
	$\omega_1$	$\omega_2$	$\alpha_R$	$\beta_R$
Hard soil	31.08	93.25	2.333	0.0008
Stiff soil	13.56	40.69	1.018	0.0018
Soft soil	8.35	25.05	0.627	0.0029

### Details on boundaries, meshing, and interface characteristics

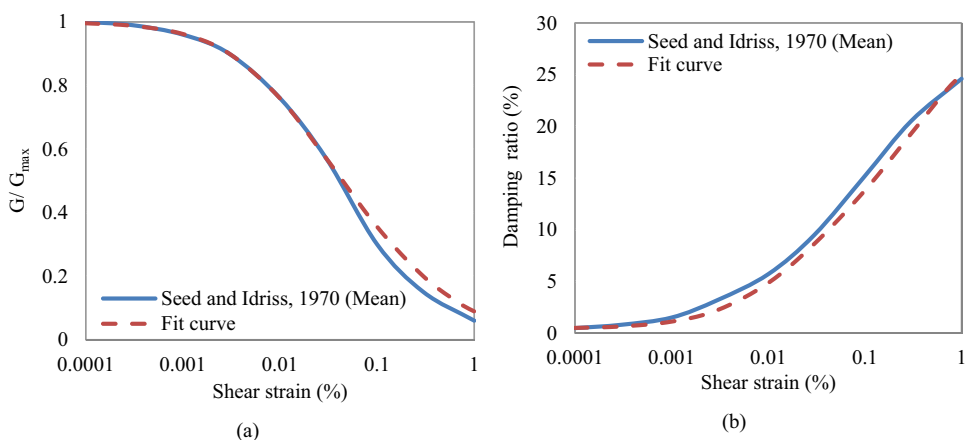
The foremost and crucial step in numerical simulation involves establishing the boundaries for a geometric model. Also, it is of utmost importance to carefully position and effectively eliminate wave reflection from the boundaries of the model. The distance between the lateral boundaries of soil models was adopted based on previous studies [46, 47]. The authors suggested the lateral boundaries be seven times the dimensions of the raft from its center, effectively minimizing wave reflection from the boundaries. Therefore, in this study, the longitudinal and lateral dimensions of the soil boundaries were adopted as 133 m and 126 m, respectively as shown in Fig. 5. The appropriate boundary conditions replicate the far-field behavior of the soil medium by absorbing stress increments and preventing the reflection of waves. Hence, employing free-field and interface elements was recommended for the dynamic analysis [63]. This study utilized free-field boundaries with viscous dampers at the lateral boundaries of the soil mediums to mitigate wave reflection and replicate energy dissipation. Lysmer and Kuhlmeyer [64] described the dependence of normal and shear stress at the boundaries on pressure and shear wave velocities as shown in Eqns. 15 and 16.

$$\sigma_{x,y} = C_1 \rho V_p u_{x,y} \tag{15}$$

$$\tau = C_2 \rho V_s u_z \tag{16}$$

where,  $\sigma_{x,y}$  = normal stress in the x or y direction, respectively,  $\tau$  = shear stress in zx or zy plane,  $\rho$  = density of soil,  $V_p$  and  $V_s$  = pressure and shear wave velocities, respectively,  $u_x$  and  $u_y$  are the nodal velocities at the boundaries in x and y directions respectively, and  $C_1$  and  $C_2$  are the relaxation coefficients were employed to formulate the absorbent boundaries at the calculation stage. Additionally, dimensionless relaxation coefficients ( $C_1$  and  $C_2$ ) were utilized to

**Fig. 4** **a**  $G/G_{max}$ —strain relationship and **b** damping—strain relationship





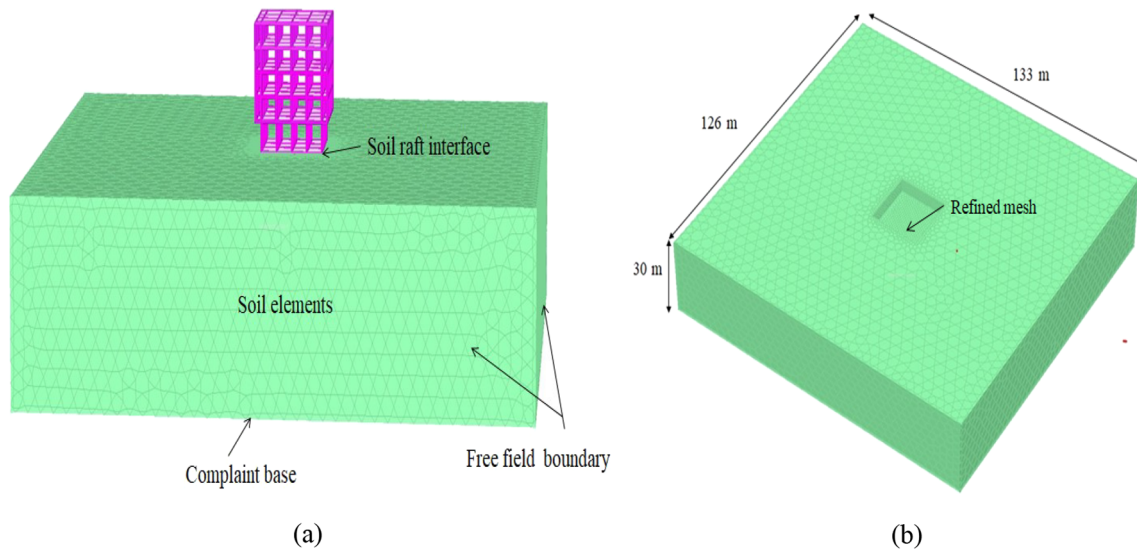


**Fig. 5** **a** Three-dimensional view structure floating column presents in XY directions, **b** solid element modeling using finite element method (PLAXIS 3D)

improve the efficiency of the wave-absorbing boundaries in the calculation phase. However, Brinkgreve et al. [65] recommended setting these coefficients as  $C_1 = 1$  and  $C_2 = 0.25$  to maintain rational shear wave transmissivity at the boundaries for dynamic SSI behavior. The bedrock level was represented by incorporating a compliant base at the bottom of the soil medium. The compliant base is combined between the viscous boundaries to mitigate the reflection of waves and enable the application of earthquake records through prescribed surface displacement. According to FEMA-273 [66], local site characteristics in the top 30 m of the soil profile stimulate earthquake amplification. Hence in this study depth of the bedrock level is considered to be 30 m below ground level.

The optimal number of elements was ascertained by conducting a mesh independence study (MIS). An MIS was conducted to investigate how the predicted response varies with the number of elements. The test was initiated with a very coarse mesh and progressed to a very fine mesh. Consequently, there is little to no significant difference in the structural response subjected to RSN-6 (Imperial Valley-02) ground motion when using a very fine mesh compared to a fine mesh. Thus, the decision was made to employ fine mesh elements for all analyses, ensuring accurate prediction of the structures dynamic response. The divided mesh comprises a total of 23,746 soil elements and 58,504 nodes, which is the highest value among all the meshed model structures. Seismic records are applied through prescribed surface displacement at the bottom of the soil model. The waves propagate through the soil medium and reach the foundation, inducing vibrations in the structure. Large concentrations of stress or deformation are expected during the analysis, especially

at the soil and foundation interaction locations. Therefore, the mesh size is reduced and locally refined around the raft foundation (with a local element refine factor of 0.125) [63], as depicted in Fig. 5b to improve structural response results. The PLAXIS three-dimensional meshing perspective for modeling soil-structure systems with floating columns in the XY directions is shown in Fig. 5. To replicate the interaction between the foundation and the surrounding soil, a strength reduction factor ( $R_{inter}$ ) was utilized within the framework of the Mohr–Coulomb failure criterion. Soil characteristics are utilized to calculate the strength reduction factor ( $R_{inter}$ ) for interfaces between structures and soil, enabling the representation of their lateral behaviors [63].

$$C_i = R_{inter} C_{soil} \tag{17}$$

$$\tan\phi_i = R_{inter} \tan\phi_{soil} \leq \tan\phi_{soil} \tag{18}$$

$$\psi_i = 0 \text{ for } R_{inter} < 1, \text{ otherwise } \psi_i = \psi_{soil} \tag{19}$$

where,  $C_i$  and  $\phi_i$  are cohesion and friction angle of the interface. The strength reduction factor ( $R_{inter}$ ) defines the roughness between the soil and the foundation. It describes the reduced shear strength at the interface between soil and foundation materials. Belinchon et al. [67] and Nor et al. [68], conducted numerical analyses using the PLAXIS finite element program to investigate interface characteristics between foundations and different soil conditions. They performed direct shear interface tests with varying strength reduction factors ( $R_{inter}$ ) ranging from 0.12 to 1 to simulate the foundation-soil interaction. Test results showed that decreasing the strength reduction factor increased soil

displacement. Thus, variations in the  $R_{\text{inter}}$  value can significantly impact the distribution of shear stress between the foundation and soil, directly affecting soil displacement. The authors, Kim et al. [69] and Fatahi and Tabatabaiefar [70] documented the utilization of a strength reduction factor of 0.75, a value commonly adopted in geotechnical practice, and found that it improved outcomes in numerical analysis. Therefore, a  $R_{\text{inter}}$  value of 0.75 is used in this study to achieve realistic results in the dynamic analysis.

## Non-linear time history analysis approach (NLTHA)

The nonlinear time-history analysis is widely regarded as the most comprehensive approach to conducting seismic analysis. At the bedrock level, the seismic force is applied by inputting an acceleration time history. The structural response is calculated continuously throughout the entire duration of an earthquake, on every second. The governing equations of motion of a structure, including its base interaction, and their solution are complicated. Hence, in this study, the direct analysis method is used to simulate the interaction of soil-raft-structure systems and solve these equations in a complex system. The direct method involves the simultaneous modeling of the soil and structures system, and it solves the dynamic equilibrium equation, as depicted in Eq. 20, in a single step.

$$[M]\{\ddot{u}\} + [C]\{\dot{u}\} + [K]\{u\} = -[M]\{\ddot{u}_g\} + \{F_{vb}\} \quad (20)$$

where,  $[M]$ ,  $[C]$ , and  $[K]$  represent the matrices for mass, viscous damping, and stiffness respectively. The vectors  $\{\ddot{u}\}$ ,  $\{\dot{u}\}$  and  $\{u\}$  refer to the acceleration, velocity, and displacement of the nodes concerning the underlying foundation. The vector  $\{F_{vb}\}$  denoted as a force vector associated with the viscous damping boundaries. Additionally,  $\{\ddot{u}_g\}$  represents the induced acceleration by seismic activity at the bedrock level [71]. In this study, the aim is to conduct a dynamic time history analysis that incorporates the nonlinearity of soil material behaviors, the inelastic behaviors of structural systems, and the consideration of cracked sections for reinforced concrete. This approach is used to evaluate the reliable response of soil-structure systems due to seismic events.

The nonlinearity of the soil material and its characteristics have been discussed in Sect. “[Hardening soil model with small strain stiffness \(HSS\) model](#)”. The geometric and material nonlinearity of structures was taken into consideration during the analysis and design of rigid-based structures. The dynamic analysis incorporated the cracking effects by assuming that cracked beams and columns were 0.35 and 0.7 times the bending stiffness of uncracked components, respectively [44]. Also, the nonlinear behavior of beam and

column structural components with lumped plasticity is taken into account by putting plastic hinges on both ends. In this study, the plastic hinge characteristics were determined by utilizing the default auto hinge properties provided by ASCE (41–17) [72]. The modes of dynamic response in which approximately 90% of the mass is involved. The damping coefficients of structures are determined by utilizing Eq. 21 and taking into account a damping ratio of 5% as described by Chopra et al. [73]. The structural characteristics and damping coefficients for all modeled structures are presented in Table 5.

$$\xi_i = \frac{1}{2} \left( \left( \frac{\alpha}{\omega_i} \right) + \beta \omega_i \right) \quad (21)$$

where  $\alpha$ ,  $\beta$ , and  $\xi$  are mass proportional coefficient, stiffness proportional damping coefficient, and critical damping ratio respectively.

## Ground motion details

The suitable ground motion records were selected based on the following factors, such as a magnitude ( $M_w$ ) range of 4.5–7.5, a source-to-site distance of 5–50 km, and the dominating frequencies according to the Indian subcontinent during the past two decades, which ranged from 0.1 to 8 Hz. The PEER (Pacific Earthquake Engineering Research) [74] database was used to collect the real strong ground motion records. This study performed the dynamic analysis incorporating a set of five acceleration time histories of earthquakes with a magnitude of above 6. The characteristics of the selected ground motion records are listed in Table 6. The selected ground motion for analysis has been appropriately scaled to IS 1893 to meet the specified pga value of 0.16 g for a moderate seismic zone.

This scaling process has been carried out using the seismomatch software [75]. According to ASCE/SEI (7–16) [2], the standard scaling procedure prevents scaled average response spectra from falling below the target spectrum over the period range of 0.2–1.5 T. Where T is the fundamental

**Table 5** Structural characteristics for all models

Type of structure	Fundamental mode frequencies (rad/s)		Rayleighs damping coefficients	
	$\omega_1$	$\omega_2$	$\alpha$	$\beta$
Without floating structure	5.13	14.30	0.3778	0.0051
Floating-X	5.40	14.27	0.3920	0.0050
Floating-Y	5.70	15.40	0.4167	0.0047
Floating-XY	4.48	13.52	0.3369	0.0054

**Table 6** Characteristics of selected ground motion

PEER No	Earthquake	Station	Predominant frequency (Hz)	$V_{s30}$ (m/s)	PGA (g)	$M_w$	$R_{jb}$ (km)	D5-95 (s)	Scale factor
6	Imperial Valley-02	El Centro array#9	2.17	213	0.2800	6.9	6.1	23.2	0.6
57	San Fernando	Castaic—Old Ridge Route	3.12	450	0.320	6.61	19.3	16.8	0.45
93	San Fernando	Whitter Narrows Dam	5.55	298	0.1070	6.61	39.5	21.5	1.52
122	Fruili-Italy-01	Codroipo	1.31	249	0.061	6.5	33.2	19	2.8
456	Morgan Hill	Gilory Array #2	4.54	270	0.162	6.19	13.7	16.6	0.98

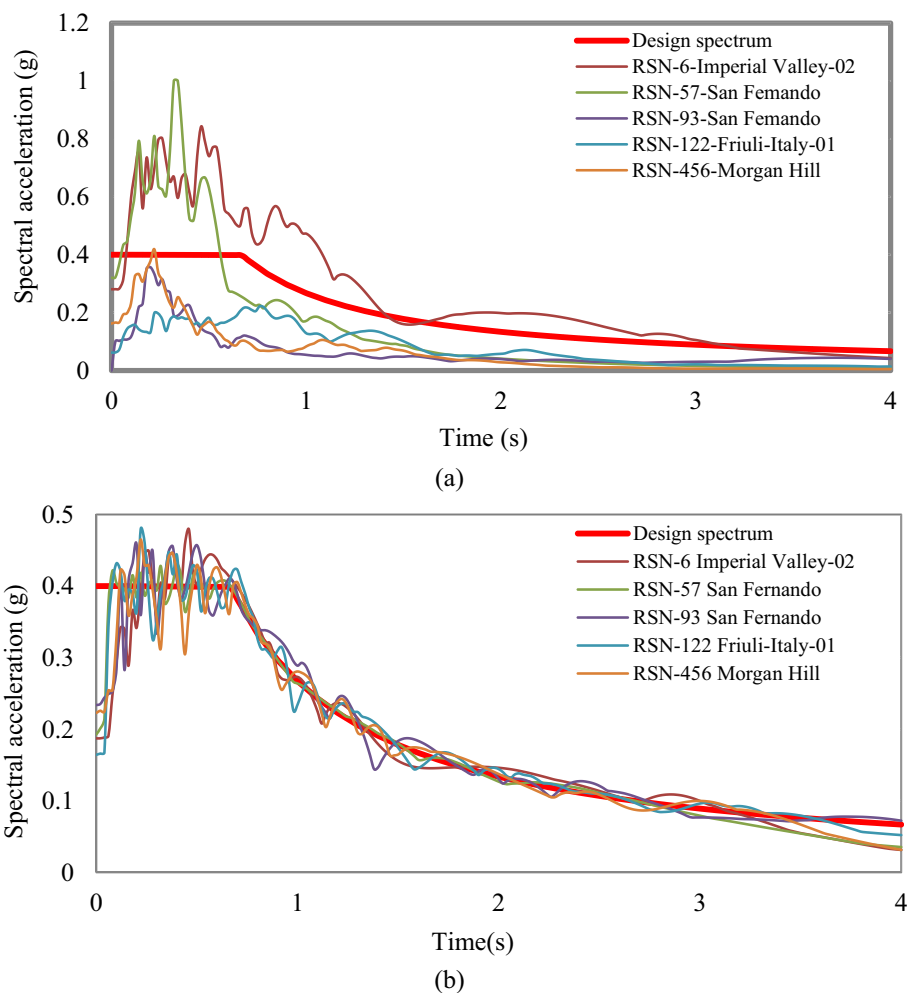
period of fixed-base structures. Over that time range, this study used a scaled ground motion average response spectrum that was not allowed to be less than the design spectrum. Bracketed duration is a common engineering way of quantifying strong ground motion. Bracket duration is the period between the first and last ground acceleration exceeding 0.05 g [76]. The bracket duration of the ground motions is applied at the rock level to perform the dynamic analysis. Figure 6 displays the unscaled and scaled response spectrum

while Fig. 7 displays the scaled acceleration time history for selected ground motions.

### Validation

The validation study involved a comparison between the results obtained from experimental and numerical simulation to evaluate the effectiveness of the nonlinear simulation.

**Fig. 6** Response spectrum for the selected ground motion for 5% damping. **a** Unscaled response spectrum, **b** scaled response spectrum



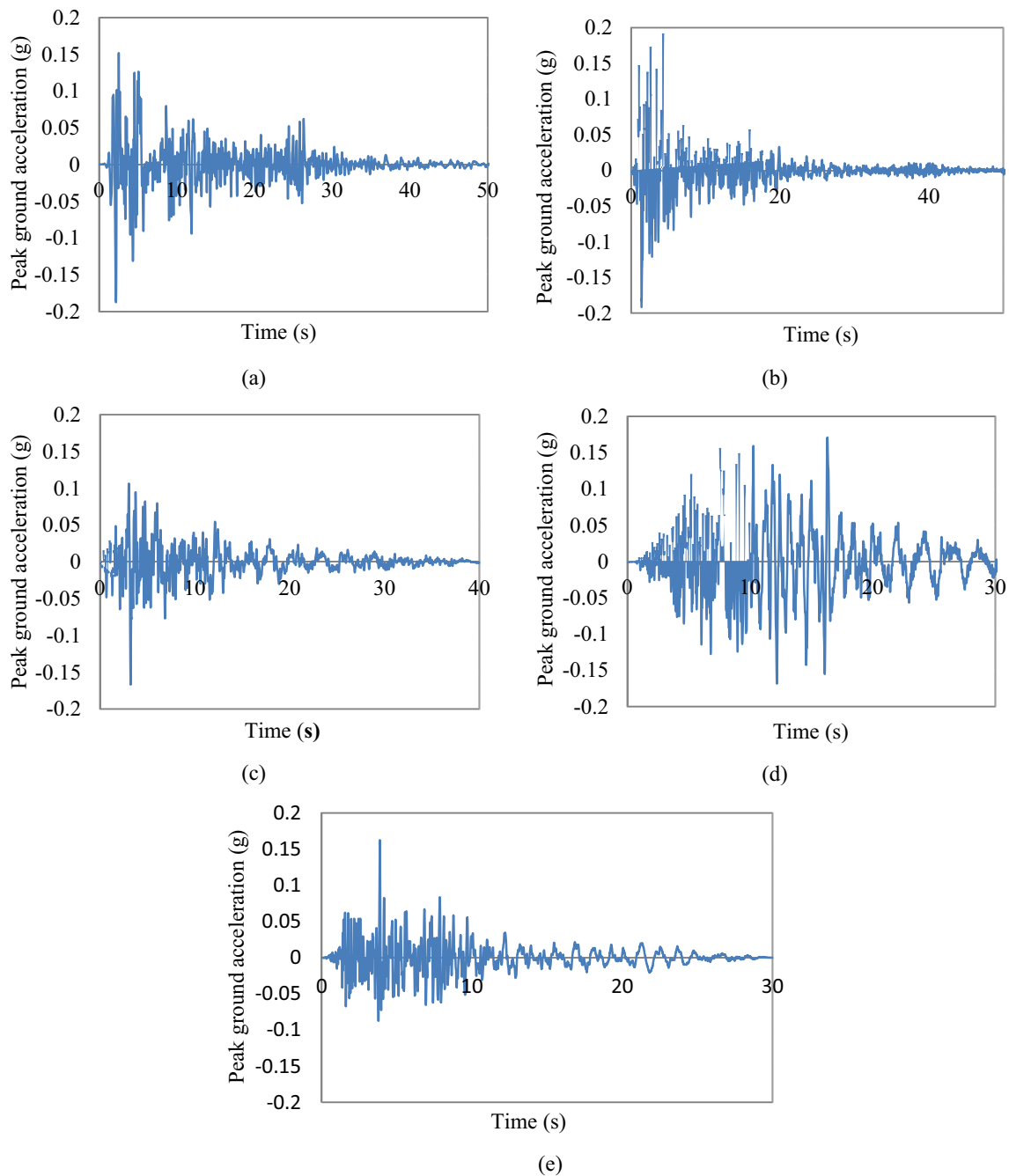


**Fig. 7** Scaled acceleration time history data for selected ground motion. **a** RSN-6 imperial valley-02, **b** RSN 57-san fernando, **c** RSN 93-san fernando, **d** RSN 122-fruiliitaly-01, and **e** RSN 456-morgan hill

El Hoseny et al. [77] conducted an experimental and numerical study on the seismic response of multistory buildings, considering SSI effects under different ground motions. For this validation investigation, a nonlinear time history analysis was performed on a prototype building frame model subjected to the Kobe earthquake of 1995. The prototype structure is composed of seven-story concrete frames supported by a raft foundation. The building frame consists of

a double bay configuration with a bay width of 4 m and a floor height of 3 m. The prototype model has a total height of 21 m. The sectional dimensions of the beam and column are  $300 \times 600$  mm and  $800 \times 800$  mm, respectively, and the slab thickness is 160 mm. The compressive strength of concrete ( $f_{ck}$ ) is 30 MPa, and the modulus of elasticity ( $E$ ) is 25,742.96 MPa. The prototype model rests on both flexible and fixed bases. The soil-foundation-structure interaction

of a real model system is shown in Fig. 8a. The soil type is silty clay with a unit weight of  $17.8 \text{ kN/m}^3$ , and the shear wave velocity ( $V_s$ ) is  $220 \text{ m/s}$ . The longitudinal and lateral boundaries of the soil model are  $70 \text{ m}$  and  $50 \text{ m}$ , respectively, and the depth soil model is  $40 \text{ m}$ . The frequency of the soil layer is  $1.375 \text{ Hz}$ . The HSS model parameters for silty clay are detailed in Table 7.

The procedure used in modeling the soil-raft-interface system remains consistent, with the same boundary

conditions and interface characteristics as discussed earlier in the HSS constitutive model section. In Fig. 8b, the numerical analysis results show absolute displacement values at the roof level for structures with fixed and flexible bases. The numerical results are  $94.2 \text{ mm}$  for fixed bases and  $103.9 \text{ mm}$  for flexible bases, while the experimental study by El Hoseny et al. [77] recorded  $92.5 \text{ mm}$  for fixed bases and  $102.5 \text{ mm}$  for flexible bases. The comparison between roof level displacement values in the numerical and experimental

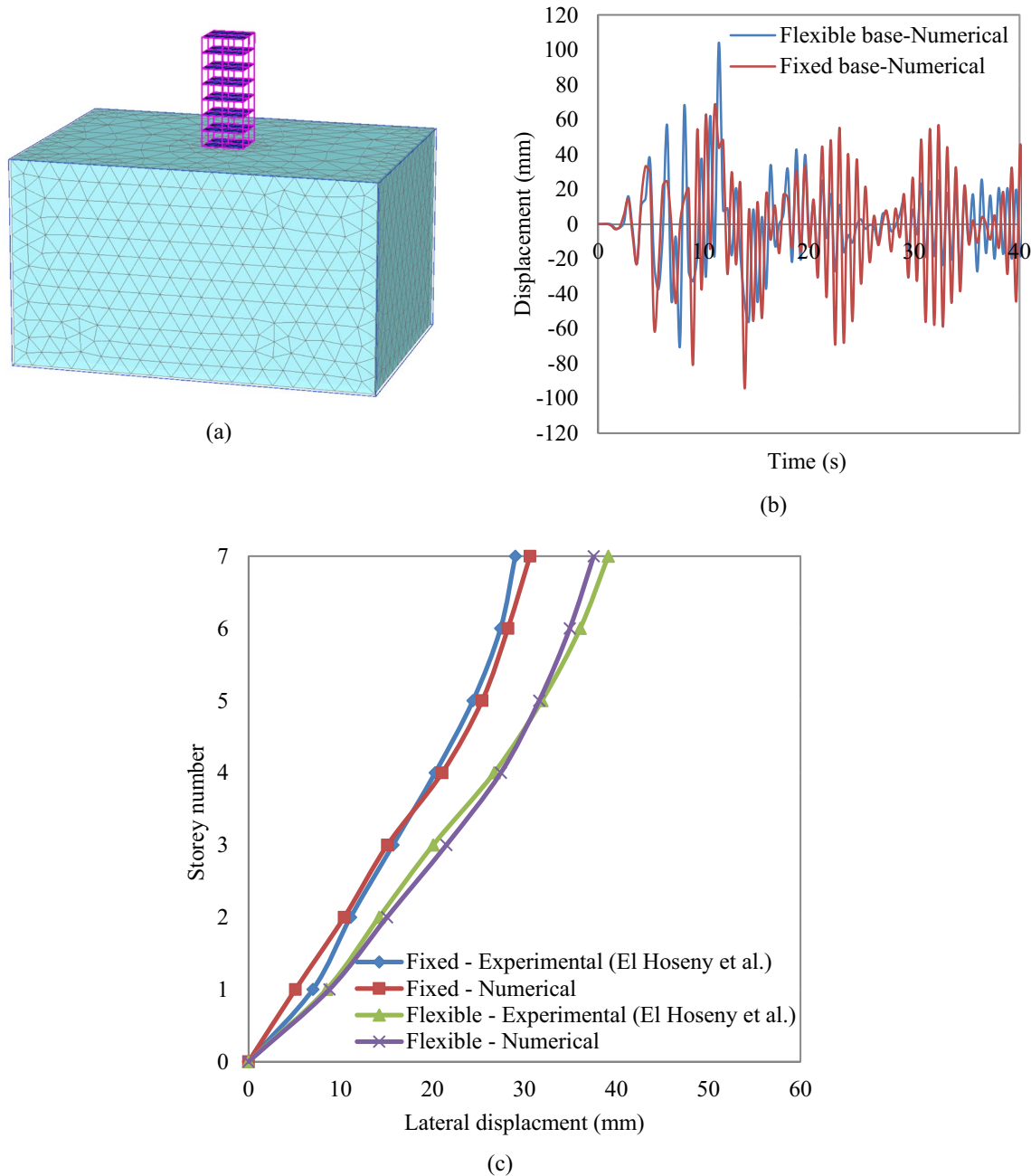


**Fig. 8** a Three-dimensional meshing view of the experimental model, b absolute displacement at roof level from numerical analysis, and c results of experimental and numerical analysis

**Table 7** Validation of relevant parameters of the HSS model

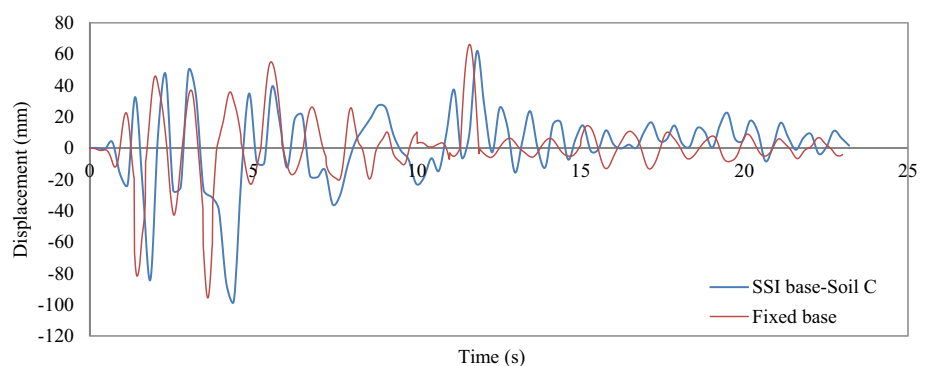
Soil type	$\gamma$ (kN/m <sup>3</sup> )	$S_u$ (kPa)	$PI$ (%)	$G_{o_{ref}}$ (MPa)	$\gamma_{0.7}$ (%)	$E_{50}^{Ref}$ (MPa)	$E_{oed}^{Ref}$ (MPa)	$E_{ur}^{ref}$ (MPa)	$\nu_{ur}$	$m$
Silty clay	21.0	76.5	18.0	82.1	0.0156	9.92	9.92	29.76	0.20	0.90

data reveals a lower percentage of errors. The comparison of relative displacement distribution between structures with fixed and flexible bases in the numerical analysis and the experimental study, as shown in Fig. 8c, demonstrates good agreement in the lateral displacement of the building.

## Result and discussion

According to the International Building Code (IBC) [48], soil C is classified as very dense and soft-rock soil. Soil C exhibits significantly greater shear wave velocity and stiffness properties. Analyzing the structural response of the soil C model in comparison to the fixed base model. The findings from both cases indicate whether the SSI (soil C) model can serve as a suitable replacement for the fixed base model. The structure floating in the XY direction was utilized to assess the seismic response of both SSI (soil C) and fixed bases subjected to RSN-6 ground motions in this check (as an example). The roof displacement of fixed and SSI (soil C) structures are compared in Fig. 9. Small differences were found between fixed and SSI (soil C) models. Thus, the soil C (SSI) model is considered a fixed base condition. In this numerical study, five-story buildings are modeled with and without floating columns located in different soil conditions, considering the soil structure interaction effect. This dynamic analysis study employed the constitutive HSS model to simulate soil nonlinear behavior and perform nonlinear time history analysis. The assessment of structural response to earthquakes involved a comparison between structures with and without floating columns incorporating the SSI effects. The results are presented in terms of the average structural responses subjected to selected five ground motions.

**Fig. 9** Roof displacement of floating column structures in XY direction due to 'RSN-6' ground motion

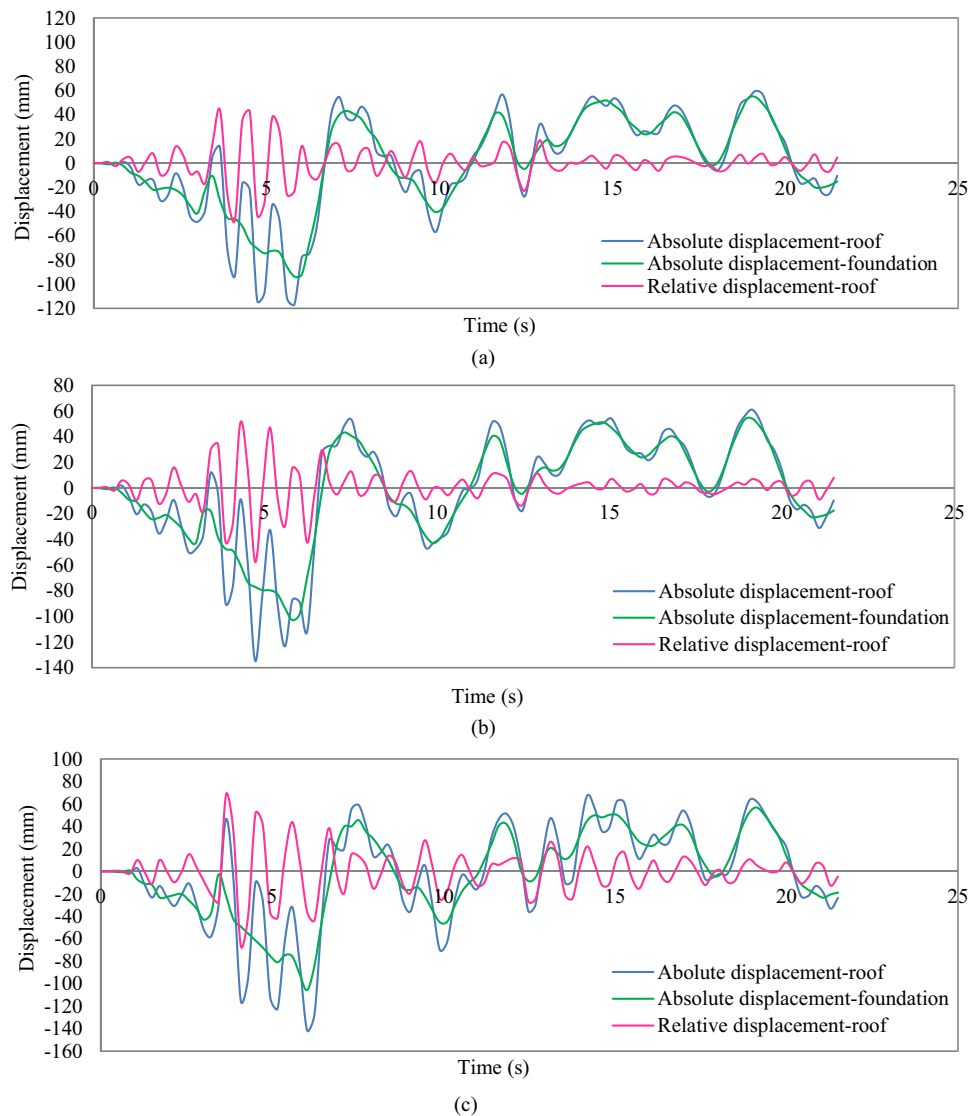


## Lateral storey displacement

The relative lateral displacement is determined by subtracting the movement at the foundation level from the movement at the storey level to assess the soil-structure interaction (SSI) effect. This section discusses the average relative lateral displacement of storey levels for all modeled structures resulting from five ground motions under different soil conditions. The structural models in this study modeled structures are considered, structures with floating columns in the X direction as FX, Y direction as FY, X, and Y directions as FXY, and without floating column structures as WOF. Figure 10 shows the absolute and relative roof level displacement of structure FXY under the San Fernando (RSN-93) ground motion in different soil conditions (as an example). The hard soil condition is considered a fixed base in Fig. 10a, the maximum absolute displacement time history at the roof level is subtracted from the foundation base to obtain a relative lateral displacement time history at the roof level. It is observed that the maximum relative displacement is  $-47$  mm, and the maximum absolute roof and foundation displacement of  $-117$  mm and  $-94$  mm respectively.

In stiff soil, Fig. 10b displays the maximum absolute displacement of the roof and foundation as  $-135$  mm and  $-103$  mm, respectively, and the relative lateral displacement at the roof level as  $-57$  mm. Figure 10c shows that on soft soil, the roof and foundation exhibited maximum absolute displacements of  $-142$  mm and  $-106$  mm, respectively. Also, the maximum relative lateral displacement was observed at  $+68$  mm. Comparing Fig. 10a–c, the amplification ratio of maximum relative lateral displacement at the roof level is the relative lateral displacement of flexible bases (stiff and soft soil) divided by fixed base (hard soil). The amplification ratio of 1.21 ( $57/47$ ) is determined under

**Fig. 10** Absolute and relative displacement time histories for the FXY model at the roof level under ‘RSN-93’. **a** Hard soil, **b** stiff soil, and **c** soft soil



stiff soil conditions. In the case of soft soil conditions, it is observed that the amplification ratio is 1.45 (68/47). Figure 11 shows the shape of the structural maximum displacement for the soil-foundation-structure system subjected to ‘RSN 93’ ground motion.

Figure 12 shows the average relative lateral displacement profile for structures with and without floating columns on different soil conditions subjected to applied ground motions at the bedrock level. The structural average relative lateral displacement at the roof level in hard soil was obtained from the analysis as shown in Fig. 12a. It is observed that the roof displacement values for different configurations such as 18 mm for WOF, 24 mm for FX, 21 mm for FY, and 29 mm for FXY structures. Roof displacements increased 1.33 times for FX, 1.17 times for FY, and 1.61 times for FXY structures compared to without floating column structure. In stiff soil conditions, WOF, FX, FY, and FXY roof displacement values were 23 mm,

33 mm, 28 mm, and 40 mm respectively (Fig. 12b). The roof displacement of structures with floating columns FX, FY, and FXY is 1.43, 1.22, and 1.74 times greater compared to structures without a floating column.

In the case of soft soil conditions, the roof displacement values for WOF, FX, FY, and FXY structures are 32 mm, 44 mm, 39 mm, and 52 mm, respectively as shown in Fig. 12c. The roof displacement values exhibit an increase of 1.37 times for FX, 1.22 times for FY, and 1.62 times for FXY in comparison to the WOF structure. The structural seismic response for both fixed and soil-structure interaction (SSI) base conditions has been significantly influenced by changes in the geometry of structures. Also, the displacement of storey levels experienced significant changes as a result of variations in the stiffness of buildings [78]. The location of floating columns in structures modifies the structural geometry and varies the structural stiffness along the height of the building. Hence, during

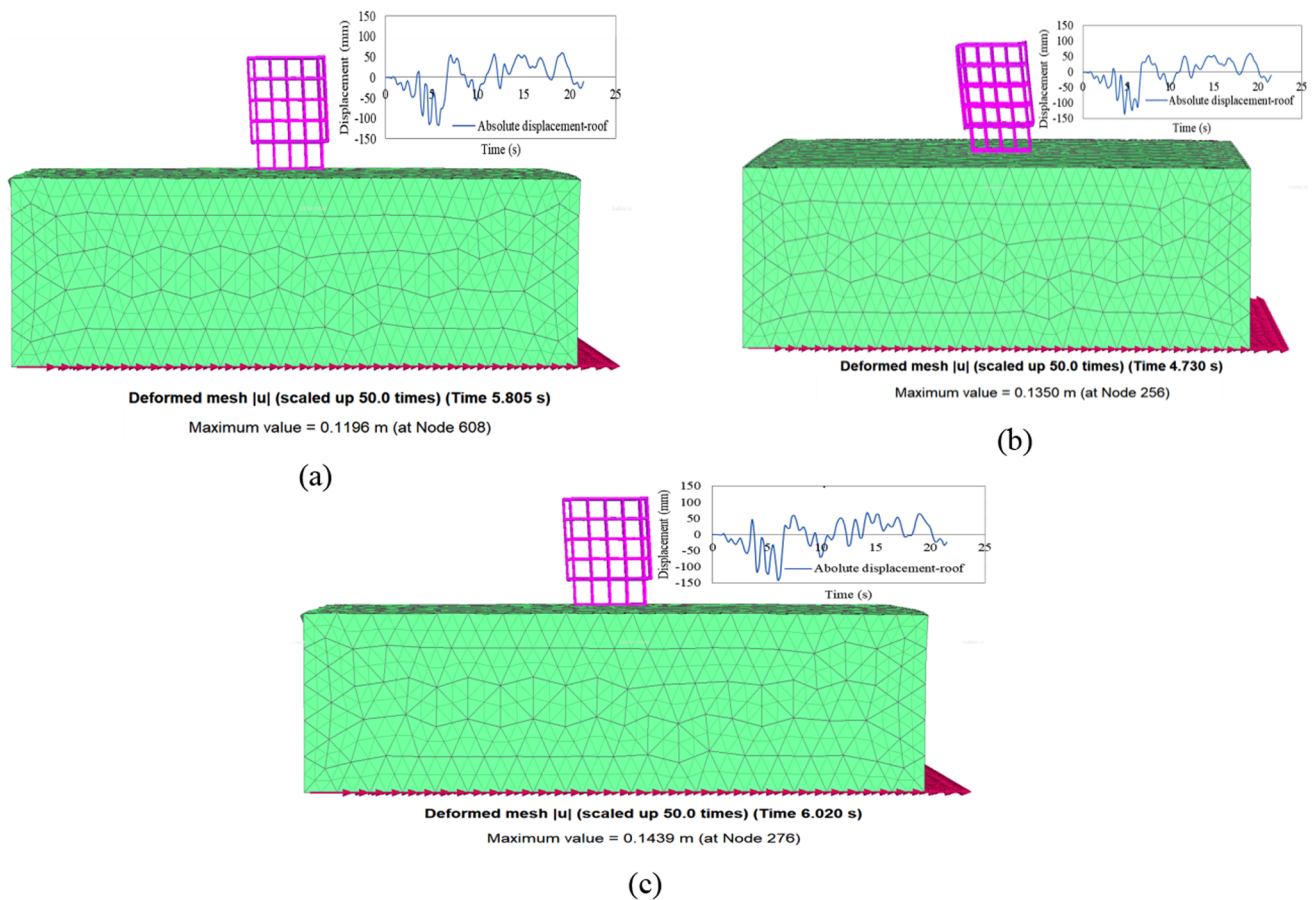


**Fig. 11** Structural maximum displacement shape for a soil-foundation-structure system subjected to ‘RSN 93’ ground motion. **a** Hard soil, **b** stiff soil, and **c** soft soil

the evaluation of structural seismic responses, one should consider the effects of structural shape under different soil conditions.

An enhanced lateral displacement occurs due to the flexibility of the soil-structure interaction. The interaction between the building and the surrounding soil allows for greater movement and deformation, resulting in increased relative lateral displacement along the height of the structure. The displacement values at the roof level in flexible bases such as stiff soil and soft soil are significantly higher than in the fixed base (hard soil) condition. The amplified value of roof displacement in stiff soil, as compared to hard soil conditions, is 1.27 times for WOF structures, 1.37 times for FX structures, 1.33 times for FY structures, and 1.38 times for FXY structures. However, in the case of soft soil condition as compared to hard soil, the observed amplified values were 1.78 times for WOF, 1.83 times for FX, 1.85 times for FY, and 1.79 times for FXY structure. Based on the analysis results, the incorporation of SSI effects enhanced the structural displacement. Specifically, structures with floating columns in the XY direction resting on soft soil

deposits significantly increase the roof displacement, which may affect building performance.

### Inter-storey drift ratio (IDR)

Storey drift ratio is the maximum relative displacement of each floor divided by its height. According to Standard Australia [79], the maximum inter-storey drift ratio is calculated using the following equation.

$$\text{Inter storey drift} = \frac{(d_{(i+1)} - d_i)}{h} \quad (22)$$

where,  $d_{(i+1)}$  = deflection at the  $(i + 1)$  level,  $d_i$  = deflection at the  $i$  level, and  $h$  = storey height. The inter-storey drift ratio is an essential structural response parameter that plays a significant role in evaluating the seismic performance of structures. It is calculated for each level, taking into account all time steps during the earthquake. The inter-storey drift ratio of the structures is supported by the fixed base (hard soil) and flexible bases (stiff and soft soil), as shown in



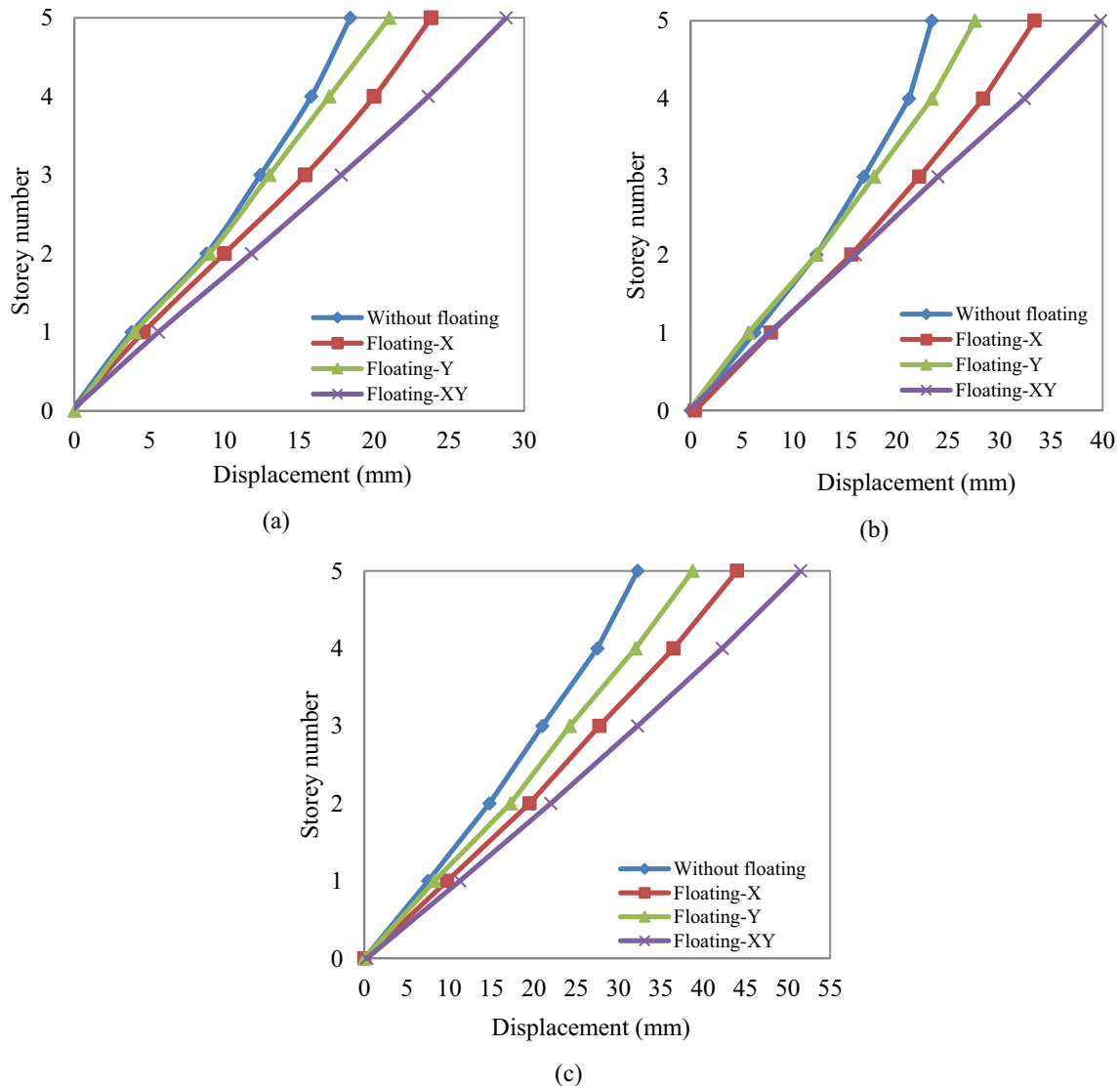


**Fig. 12** Distribution of average relative lateral storey displacement. **a** Hard soil, **b** stiff soil, and **c** soft soil

Fig. 13a–c. The orientation of floating columns in structures has been found to alter the inter-storey drift ratio when compared to those without floating column structures. Table 8 provides a summary of the maximum inter-storey drift ratios for both types of structures.

The analysis results reveal that floating column structures have an increasing inter-storey drift ratio in fixed base (hard soil) conditions, with values increasing by 7% for FX and FY structures and 28% for FXY structures compared to WOF structures. In flexible bases, the structures floating columns (FX, FY, and FXY) have higher values in stiff soil conditions (29%, 12%, and 41%), and soft soil conditions (27%, 18%, and 40%) compared to without floating column structures. In addition, it is important to note the significant increase in IDR values for structures with floating columns

(FX, FY, and FXY) compared to those without floating column structures.

When SSI effects are incorporated into flexible base models instead of fixed base models, the inter-storey drift values of structures are amplified. In stiff soil conditions, flexible base structures have an increasing percentage of IDR values are 21%, 46%, 26%, and 33% for structures WOF, FX, FY, and FXY, respectively, compared to fixed base structures. Additionally, compared to fixed base structures, soft soil conditions have a greater effect on structures with WOF, FX, FY, and FXY by 57%, 86%, 73%, and 72%, respectively. These findings reveal that the presence of SSI effects significantly amplifies the inter-storey drift values of structures, particularly in soft soil conditions. The decreasing dynamic characteristics of the subsoil conditions, which increase the

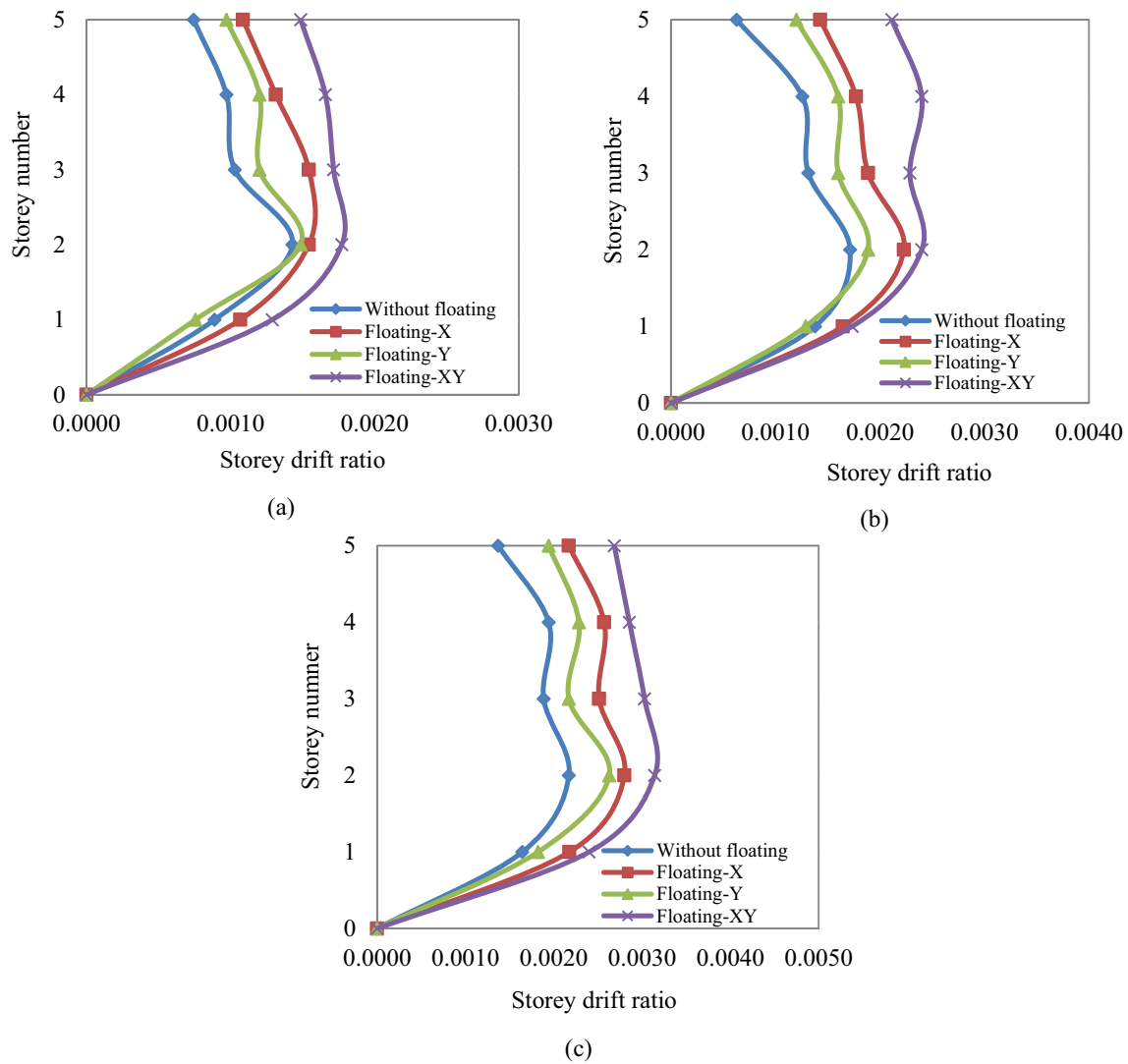


Fig. 13 Distribution of storey drift. a Hard soil, b stiff soil, c soft soil

Table 8 Maximum inter storey drift values of structures resting on different soil medium

Soil type	Inter storey drift (IDR) values			
	Without floating column structures (WOF)	Floating columns structure in X direction (FX)	Floating columns structure in Y direction (FY)	Floating columns structure in XY direction (FXY)
Hard soil	0.0014	0.0015	0.0015	0.0018
Stiff soil	0.0017	0.0022	0.0019	0.0024
Soft soil	0.0022	0.0028	0.0026	0.0031

lateral displacement of buildings, are the cause of fluctuating inter-storey drift ratios between fixed and flexible bases.

This study has shown that the presence of SSI can lead to an uneven distribution of inter-storey drift ratios, with higher values observed in the middle stories compared to the top and bottom levels. In addition, the inter-storey height,

defined as the ratio between ground and typical ground storey height, is 1.285 (4.5 / 3.5). However, the variations in height between floor levels affect the stiffness and strength of each storey. An increased ground storey height increases the drift ratio above the changed storey, while top story drift decreases. It is evident, according to the Ghoozhdi et al. [22]

study, that changing the ground floor height increases the drift ratio immediately above modified storey levels and decreases at top levels.

### Peak horizontal acceleration (PHA)

The horizontal acceleration response at the roof level of structures with floating columns oriented in the XY direction (FXY) resting on various soil types subjected to ground motion “RSN 57” (as an example) is shown in Fig. 14. Peak horizontal acceleration at the level of FXY buildings is  $4.81 \text{ m/s}^2$ ,  $3.81 \text{ m/s}^2$ , and  $3.70 \text{ m/s}^2$  for hard, stiff, and soft soil conditions, respectively. The study reveals that the peak horizontal acceleration at the roof level decreases by 21% and 23% in stiff and soft soil conditions compared to hard soil conditions. The findings of the study indicate that buildings resting on hard soil conditions experience higher peak horizontal acceleration at roof level compared to those on stiff and soft soil conditions. This decrease in peak horizontal acceleration at the roof level suggests that the stiffness of the soil has a significant impact on the structural response.

Figure 15, shows the highest horizontal acceleration amplification ( $PHA_{\text{storey}}/PHA_{\text{bedrock}}$ ) occurs at the roof level for all structural models in different soil conditions. For WOF, FX, FY, and FXY structures, the roof level amplification is 5.10, 5.5, 5.32, and 5.80 times higher than the bedrock acceleration in hard soil conditions, as shown in Fig. 15a. In stiff soil conditions, the amplified values are 3.99, 4.28, 4.10, and 4.74, respectively, as shown in Fig. 15b. In the case of soft soil conditions, the roof acceleration amplifications are 2.71, 2.98, 2.83, and 3.16, respectively as shown in Fig. 15c.

In comparing the fixed base model on hard soil to flexible base models in stiff and soft soil conditions, it was found that the amplification ratio was higher for the fixed base model. However, the interaction models showed that incorporating the nonlinear behavior of soil in the model led to more consistent changes in the building height compared to the fixed base model. It was evident that the incorporation of SSI effects in moment-resisting frame buildings significantly

lowered horizontal acceleration values at the roof level as compared to fixed-base model structures [80, 81].

### Base shear value and internal forces in members due to seismic load

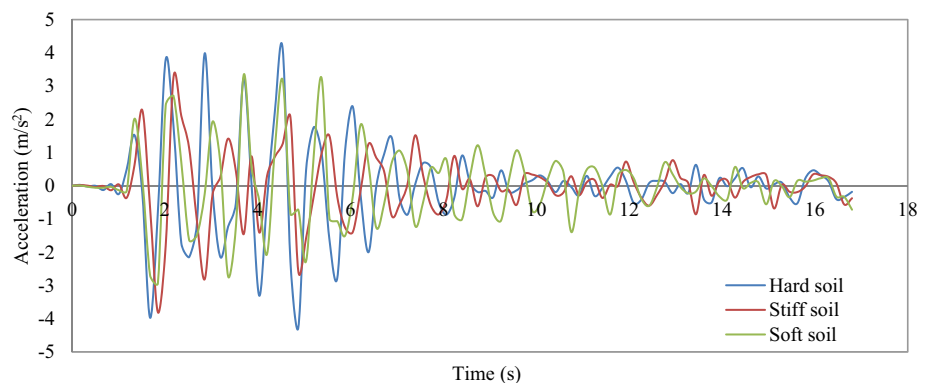
The ultimate response of the base shear in each model is calculated by combining the maximum shear force in the ground floor columns during five earthquake excitations [43]. The results regarding the ultimate response of the base shear under the five selected seismic records are presented in Table 9. The result of the time history analysis of models reveals that incorporating the SSI effect reduced the base shear value of structures. When compared to models with fixed bases (hard soil), the flexible bases (stiff and soft soil) in each model significantly reduced the base shear value. In comparison to fixed base models, the reduction in base shear for all models with flexible bases ranges from 46 to 60% for stiff soil conditions to 66 to 75% for soft soil conditions.

The envelope in Table 10 shows the maximum bending moment values for the selected beams highlighted in Fig. 16. Comparing envelopes, flexible base models exhibit higher bending moments than fixed base models. Bending moments caused by varying base settlement due to soil-structure interaction decrease from the bottom to the top of structures. The ultimate response of axial forces and moments in the studied column (Fig. 16) when subjected to five ground motions is presented in Table 11. Comparing these envelopes reveals notably higher axial forces in the flexible base model under both stiff and soft soil conditions compared to the fixed base (hard soil) model. Conversely, there was a decrease in bending moment values in the beams of flexible base models compared to fixed base models.

### Conclusion

This study examines a comprehensive numerical analysis of the seismic response of mid-rise reinforced concrete structures, both with and without floating columns,

**Fig. 14** Comparison of roof level acceleration history of FXY structures under different soil conditions subjected to ground motion “RSN 57”



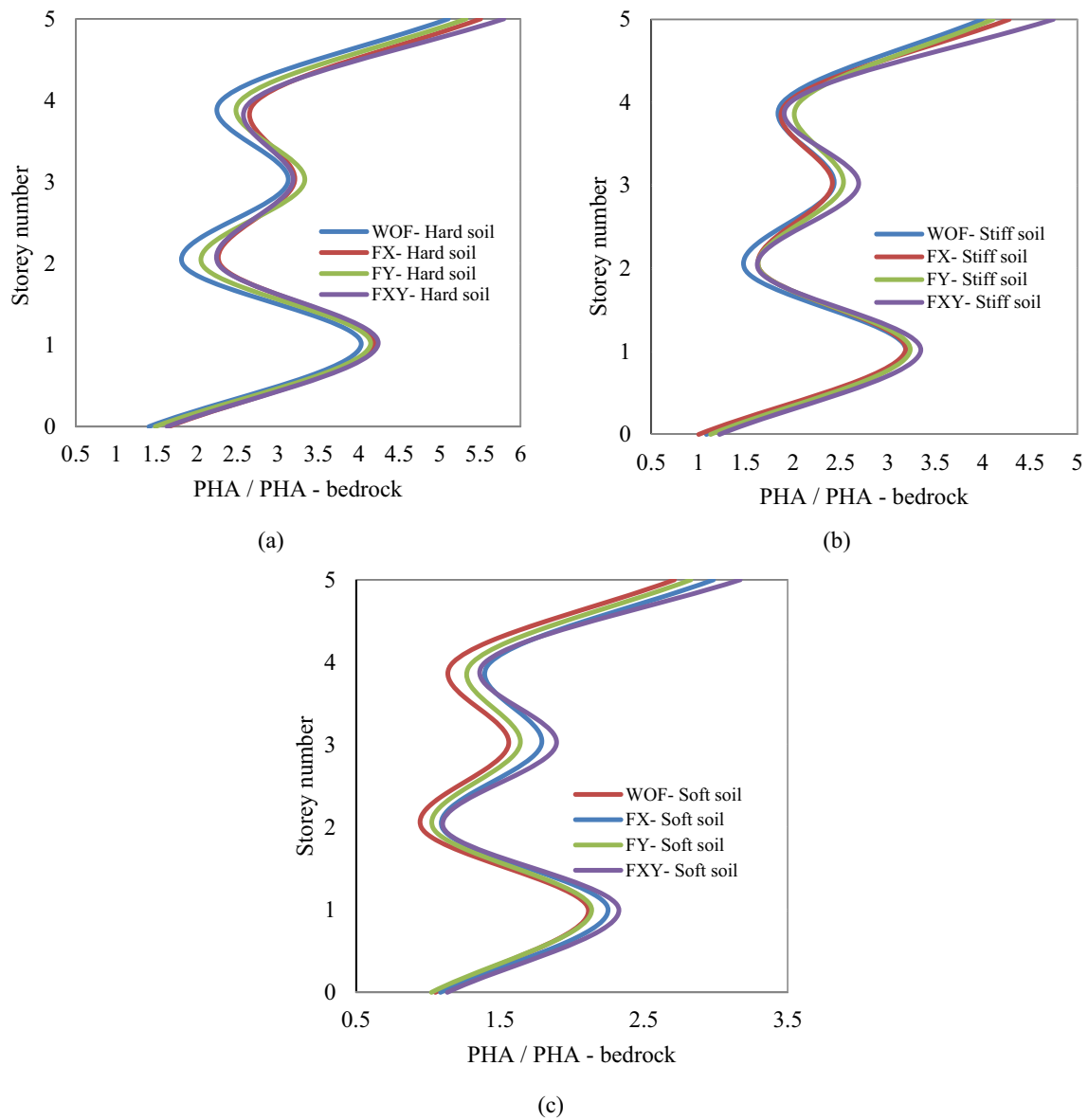


**Fig. 15** Ratio of structure PHA to bedrock PHA. **a** Hard soil, **b** stiff soil, **c** soft soil

**Table 9** Ultimate response of base shear response to five selected earthquake motions

Soil type	Base shear (t)			
	Structure type			
	WOF	FX	FY	FXY
Hard soil	119.8	174.3	152.6	184.1
Stiff soil	64.0	72.5	68.2	73.3
Soft soil	40.6	42.8	42.4	51.3

taking into account the effects of soil-structure interaction (SSI). Structures with floating columns were considered in different configurations (X, Y, and XY). Three different

types of soil conditions (hard, stiff, and soft) were taken into account in this study. The PLAXIS 3D finite element programming tool was used to simulate the interaction between soil and structure, employing the direct method. Nonlinear time history analysis was conducted to assess the seismic response of structures subjected to selected ground motions. The study assesses key seismic response parameters such as peak lateral displacement, peak inter-storey drift ratio, peak horizontal acceleration, base shear, and member forces for different structural configurations and soil conditions. The findings from the nonlinear dynamic analysis of this study can be summarized as follows.

**Table 10** The ultimate response of the bending moment in the chosen beam

Structure type	Maximum bending moment (t-m)								
	Beam-1			Beam-2			Beam-3		
	Hard	Stiff	Soft	Hard	Stiff	Soft	Hard	Stiff	Soft
WOF	3.88	4.40	4.81	1.79	2.90	4.26	0.9	1.33	1.44
FX	5.44	5.44	5.68	1.81	3.44	3.98	1.24	1.29	1.59
FY	4.05	4.49	4.9	1.90	3.30	4.17	1.15	1.79	1.58
FXY	4.56	5.59	6.81	1.95	3.47	5.07	1.87	2.18	2.84

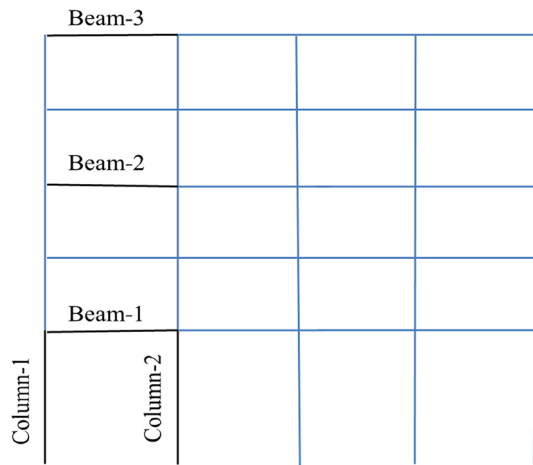


**Fig. 16** Locations of studied columns and beams

(a) The incorporation of soil-structure interaction in non-linear dynamic analysis results for flexible base structures (stiff and soft soil) reveals that lateral storey displacement significantly increases compared to fixed base (hard soil) structures. In stiff soil conditions, peak lateral displacement increases by 1.27 to 1.38 times for all modeled structures. In soft soil conditions, this effect is even more pronounced, with increases ranging from 1.78 to 1.85 times. Specifically, structures with floating columns in an XY configuration resting on soft soil deposits exhibit the highest roof displacement when subjected to earthquake excitation.

- (b) The orientation of floating columns in structures significantly influences the structural seismic response, enhancing it through variations in geometry and structural stiffness across the building height. Notably, in structures with floating columns (FX, FY, and FXY) resting on soft soil deposits, the lateral roof displacement increased by 1.22 to 1.62 times compared to structures without floating columns.
- (c) The incorporation of soil-structure interaction (SSI) effects in the analysis results in amplified inter-story drift values in flexible base structures (stiff and soft soil) compared to fixed base (hard) structures. In stiff soil conditions, inter-story drift increases by 21% to 46% for all modeled structures. In soft soil conditions, this effect is even more pronounced, with increases ranging from 57 to 86%. It is noteworthy that structures with floating columns consistently exhibit higher inter-story drift ratios in all soil mediums compared to those without floating column structures.
- (d) The amplified peak horizontal acceleration in all structural models reached its maximum at the roof level. The ratio of peak horizontal acceleration at the storey level to peak horizontal acceleration at the bedrock was higher in hard soil conditions compared to stiff and soft soil conditions.
- (e) Incorporating soil-structure interaction (SSI) effects in the analysis results in a significant reduction in base shear values. Flexible base models (stiff and soft soil) demonstrate a substantial decrease in base shear compared to fixed base models (hard). The reduction

**Table 11** Peak axial forces and bending moments in chosen columns

Structure type	Axial forces (t)						Bending moment(t-m)					
	Column-1			Column-2			Column-1			Column-2		
	Hard	Stiff	Soft	Hard	Stiff	Soft	Hard	Stiff	Soft	Hard	Stiff	Soft
WOF	42.7	47.2	62.4	34.3	40.7	48.1	6.63	5.24	3.803	5.712	3.61	2.893
FX	43.8	61.8	92	52.1	48.6	54.1	7.82	7.8	5.372	6.24	4.02	3.103
FY	66.8	67.2	95.3	51.2	66.4	75.8	7.65	7.3	5.55	6.01	3.65	2.465
FXY	78.6	70.2	109.4	69.6	81.68	74.2	7.413	7.35	5.64	7.12	4.219	3.291

obtained ranges from 46 to 60% in stiff soil and from 66 to 75% in soft soil.

- (f) Bending moments in the studied beams and axial forces in columns show significant increases in flexible base models during earthquakes.

This numerical study finding reveals that the incorporation of soil-structure interaction affects soil foundation flexibility and significantly influences building seismic demand. Neglecting the SSI effects may result in underestimated responses and increased seismic risks. The floating column structures located in seismic-prone areas are more vulnerable especially structures resting on soft soil deposits. Hence, it is important to ensure the safety of floating column structures, even in moderately seismic areas, needs proper attention and the implementation of effective retrofitting methods to prevent potential failures. The current study focuses solely on the seismic response of floating column structures outside regular buildings on homogeneous soil conditions. The authors suggest further studies incorporating the SSI effects on the dynamic behaviors of floating column structures with different heights and shapes of buildings resting on heterogeneous multilayered soil conditions. Additionally, exploring the impact of floating columns inside buildings at different floor levels is recommended. Adopting suitable retrofitting methods to mitigate the seismic vulnerability of structures is also suggested.

**Author contributions** PJ: conceptualization, methodology, numerical investigation, validation, writing, and original draft preparation JAV: conceptualization, supervision, writing, reviewing, and editing. All authors have read and agreed to the published version of the manuscript.

## Declarations

**Conflict of interest** The authors declare that they have no known competing financial interests or personal relationships that could have appeared to influence the work reported in this paper.

**Ethical approval** This article does not contain any studies with human participants or animals performed by any of the authors.

**Informed consent** For this type of study, no informed consent is required.

## References

- Kramer SL (1996) Geotechnical earthquake engineering. Pearson Education India
- Minimum Design Loads and Associated Criteria For Buildings and Other Structures (2016) ASCE/SEI 7, Reston
- FEMA P-1050 (2015) NEHRP recommended seismic provisions for new buildings and other structures. Washington
- IS: 1893 (Part I) (2002) Indian standard criteria for earthquake resistant design of structures, fifth revision, Part-1. Bureau of Indian Standards, New Delhi
- Stewart JP, Seed RB, Fenves GL (1999) Seismic soil-structure interaction in buildings. II: Empirical findings. *J Geotech Geoenviron Eng* 125(1):38–48
- Galal K, Naimi M (2008) Effect of soil conditions on the response of reinforced concrete tall structures to near-fault earthquakes. *Struct Des Tall Special Build* 17(3):541–562
- Veletsos AS, Meek JW (1974) Dynamic behaviour of building-foundation systems. *Earthquake Eng Struct Dynam* 3(2):121–138
- Jennings PC, Bielak J (1973) Dynamics of building-soil interaction. *Bull Seismol Soc Am* 63(1):9–48. <https://doi.org/10.1785/bssa0630010009>
- Bhattacharya K, Dutta SC, Dasgupta S (2004) Effect of soil flexibility on dynamic behaviour of building frames on raft foundation. *J Sound Vib* 274(1–2):111–135
- Abdel Raheem SE, Ahmed MM, Alazrak TM (2014) Soil-raft foundation-structure interaction effects on seismic performance of multi-story MRF buildings. *Eng Struct Technol* 6(2):43–61
- Kant R, Al Agha W, Almorad WA, Thakur MS, Umamaheswari N (2022) Study on seismic performance of reinforced concrete multi-storey building considering soil-structure interaction effect. *Mater Today: Proc* 56:2158–2166
- Scarfone R, Morigi M, Conti R (2020) Assessment of dynamic soil-structure interaction effects for tall buildings: a 3D numerical approach. *Soil Dyn Earthq Eng* 128:105864. <https://doi.org/10.1016/j.soildyn.2019.105864>
- Jaber L, Temsah Y, HageChehade F, El-Mossallamy Y (2018) Effect of soil-structure interaction constitutive models on dynamic response of multi-story buildings. *J Eng Sci Technol Rev* 11(3):56–60
- Gouasmia A, Djeghaba K (2006) Effects of nonlinear dynamic soil-structure interaction on the response of buildings. *Res J Appl Sci* 1(1–4):110–115
- Ghandil M, Behnamfar F (2015) The near-field method for dynamic analysis of structures on soft soils including inelastic soil-structure interaction. *Soil Dyn Earthq Eng* 75:1–17. <https://doi.org/10.1016/j.soildyn.2015.03.018>
- Uniform Building Code (1997) In Uniform building code. International Conference of Building Officials
- FEMA: 450 (Part I) (2003) NEHRP Recommended provisions for seismic regulations for new buildings and other structures
- Eurocode 8 (2005) Design of structures for earthquake resistance-part 1: general rules, seismic actions, and rules for buildings. European Committee for Standardization
- Moehle JP (1984) Seismic response of vertically irregular structures. *J Struct Eng (NY)* 110(9):2002–2014. [https://doi.org/10.1061/\(asce\)0733-9445\(1984\)110:9\(2002\)](https://doi.org/10.1061/(asce)0733-9445(1984)110:9(2002))
- Athanassiadou CJ (2008) Seismic performance of R/C plane frames irregular in elevation. *Eng Struct* 30(5):1250–1261. <https://doi.org/10.1016/j.engstruct.2007.07.015>
- Ravikumar CM, Babu Narayan KS, Sujith BV, Venkat Reddy D (2012) Effect of irregular configurations on seismic vulnerability of RC buildings. *Archit Res* 2(3):20–26
- Asadi Ghoozhdi H, Attarnejad R, Masoodi AR, Majlesi A (2022) Seismic assessment of irregular RC frames with tall ground story incorporating nonlinear soil-structure interaction. *Structures* 41:159–172. <https://doi.org/10.1016/j.istruc.2022.05.001>
- Sabari S, Praveen JV (2014) Seismic analysis of multistorey building with floating column. *Int J Civil Struct Eng Res* 2(2):12–23
- Singla S, Rahman A (2015) Effect of floating columns on seismic response of multi-storeyed RC framed buildings. *Int J Eng Res Technol* 4:1131–1136

25. Pardhi A, Shah P, Satishyadav PS, Jha AK (2016) Seismic analysis of rcc building with and without floating columns. *Int J Adv Technol Eng Sci* 4(3):615–621
26. Prasannan P, Mathew A (2017) Seismic performance of RC floating column considering different configurations. *Int J Eng Res Technol* 6(5):100–108
27. Pawar N, Dabhekar K, Patil P, Khedikar I, Jaju S (2021) Effect of floating columns on buildings subjected to seismic forces. *IOP Conf Ser: Mater Sci Eng* 1197(1):012018
28. Ibrahim A, Askar H (2021) Dynamic analysis of a multistory frame RC building with and without floating columns. *Am J Civ Eng* 9(6):177
29. Rangwala MA, Singh SK (2018) Seismic analysis of multistorey frame with and without floating columns. *Int J Innov Res Sci Eng Technol* 7(5):5262–5272
30. Nanabala SG, Ramancharla PK, Arunakanthi E (2014) Seismic analysis of a normal building and floating column building. *Int J Eng Res Technol* 3(9):981–987
31. Jagan P, Visuvasam JA (2022) Inelastic seismic behaviour of RC buildings with floating columns considering soil-structure interaction. *Symp Earthq Eng Springer Nat* 2:313–324
32. Bhosale AS, Davis R, Sarkar P (2017) Vertical irregularity of buildings: Regularity index versus seismic risk. *ASCE-ASME J Risk Uncertain Eng Syst Part A: Civil Eng* 3(3):04017001. <https://doi.org/10.1061/ajrua6.0000900>
33. Shashikumar NS, Gowda MR, Ashwini BT, Kumar YMV (2018) Seismic performance of braced framed structure with floating column. *Int J Sci Dev Res* 3(6):388–405
34. Kapase R, Pawar M, Deshmukh MM, Talavara SB (2017) Effect of seismic retrofitting on RC building with soft storey and floating column. *Int J Eng Trends Technol* 46(7):367–371
35. Kumbhar G, Banhatti A (2016) Seismic retrofitting of building with soft storey and floating column. *Int Res J Eng Technol* 3(7):1917–1921
36. Singh N, Kashyap V (2016) Seismic retrofitting of dormitory buildings with soft storey and floating columns. *Int Res J Eng Technol* 5(12):102–113
37. Saeed A, Najm HM, Hassan A, Qaidi S, Sabri MMS, Mashaan NS (2022) A comprehensive study on the effect of regular and staggered openings on the seismic performance of shear walls. *Buildings* 12(9):1293
38. Ozkılıc YO, Karalar M, Aksoylu C, Beskopylny AN, Stelmakh SA, Shcherban EM, Azevedo AR (2023) Shear performance of reinforced expansive concrete beams utilizing aluminium waste. *J Market Res* 24:5433–5448
39. Tayeh BA, Akeed MH, Qaidi S, Bakar BA (2022) Influence of the proportion of materials on the rheology and mechanical strength of ultrahigh-performance concrete. *Case Stud Constr Mater* 17:e01433
40. IS: 456 (2000) Plain and reinforcement concrete code of practice. Bureau of Indian Standards, New Delhi, India
41. IS: 875 (Part 2) (1987) Code of practice for design loads (other than earthquake) for buildings and structures—imposed loads
42. Roy T, Saito T, Matsagar V (2021) Multihazard framework for investigating high-rise base-isolated buildings under earthquakes and long-duration winds. *Earthq Eng Struct Dynam* 50(5):1334–1357
43. Shabani MJ, Shamsi M, Ghanbari A (2021) Seismic response of RC moment frame including topography–soil–structure interaction. *Pract Period Struct Des Constr* 26(4):04021046
44. IS: 1893 (Part I) (2016) Indian standard criteria for earthquake resistant design of structures, fifth revision, Part-I. Bureau of Indian Standards, New Delhi
45. Sap 2000 (Version 8) (2002) Integrated software for structural analysis and design. Computers and Structures Inc.
46. Kumar M, Mishra SS (2016) Study of seismic response characteristics of building frame models using shake table test and considering soil structure interaction. *Asian J Civil Eng* 20(3):409–419
47. Visuvasam J, Chandrasekaran SS (2019) Effect of soil–pile–structure interaction on seismic behaviour of RC building frames. *Innov Infrastruct Solut* 4(1):45
48. International Building Code (2008) International Code Council, USA
49. Uma Maheswari R, Boominathan A, Dodagoudar GR (2010) Use of surface waves in statistical correlations of shear wave velocity and penetration resistance of Chennai soils. *Geotech Geol Eng* 28(2):119–137. <https://doi.org/10.1007/s10706-009-9285-9>
50. Bowles J.E (1996) Foundation analysis and design, 5th edn. McGraw-Hill Education (ISE Editions)
51. Peck RB, Hanson WE, Thornburn TH (1974) Foundation engineering, 2nd edn, John Wiley & Sons
52. Schanz T, Vermeer PA, Bonnier PG (1999) The hardening soil model: formulation and verification, beyond 2000 in computational geotechnics, 1: 281–296
53. Plaxis BV (2022) Plaxis material models manual, The Netherlands
54. Hejazi Y, Dias D, Kastner R (2008) Impact of constitutive models on the numerical analysis of underground constructions. *Acta Geotech* 3(4):251–258. <https://doi.org/10.1007/s11440-008-0056-1>
55. Hardin BO, Drnevich VP (1972) Shear modulus and damping in soils: Design equations and curves. *J Soil Mech Found Div* 98(7):667–692
56. Cerfontaine B, Knappett JA, Brown MJ, Bradshaw AS (2019) Effect of soil deformability on the failure mechanism of shallow plate or screw anchors in sand. *Comput Geotech* 109:34–45. <https://doi.org/10.1016/j.compgeo.2019.01.007>
57. Daredndeli (2001) Development of a new family of normalized modulus reduction and material damping curves, Ph.D. Dissertation, The University of Texas at Austin, Texas
58. Amorosi A, Boldini D, Di Lernia A (2016) Seismic ground response at Lotung: hysteretic elasto-plastic-based 3D analyses. *Soil Dyn Earthq Eng* 85:44–61
59. Fatahi B, Huang B, Yeganeh N, Terzaghi S, Banerjee S (2020) Three-dimensional simulation of seismic slope–foundation–structure interaction for buildings near shallow slopes. *Int J Geomech* 20(1):04019140. [https://doi.org/10.1061/\(asce\)gm.1943-5622.0001529](https://doi.org/10.1061/(asce)gm.1943-5622.0001529)
60. Rizzitano S, Cascone E, Biondi G (2014) Coupling of topographic and stratigraphic effects on seismic response of slopes through 2D linear and equivalent linear analyses. *Soil Dyn Earthq Eng* 67:66–84. <https://doi.org/10.1016/j.soildyn.2014.09.003>
61. Hashash YMA, Musgrove MI, Harmon JA (2018) Nonlinear and equivalent linear seismic site response of one-dimensional soil columns. *User Manual v7. 0, Deepsoil Software* 12(10)
62. Seed H, Wong RT, Idriss IM, Tokimatsu K (1986) Moduli and damping factors for dynamic analyses of cohesionless soils. *J Geotech Eng* 112(11):1016–1032
63. Plaxis BV (2022) Plaxis reference manual. The Netherlands
64. Lysmer J, Kuhlemeyer RL (1969) Finite dynamic model for infinite media. *J Eng Mech Div* 95(4):859–877
65. Brinkgreve R, Swolfs WM, Engine E (2010) PLAXIS 2D dynamic version
66. FEMA: 273 (1997) NEHRP guidelines for the seismic rehabilitation of buildings, Federal Emergency Management Agency
67. Belinchon P, Sorensen KK, Christensen R (2016) A case study of the interaction between a pile and soft soil focusing on negative skin friction using finite element analysis. In: *Proc 17th Nord Geotech Meet*, pp 513–522

68. Mat Nor AH, Yahuda AH, Pakir F (2014) Analysis of lightweight concrete “CakarAyam” foundation for road construction using Plaxis 3D foundation software. *Appl Mech Mater* 695:729–733. <https://doi.org/10.4028/www.scientific.net/amm.695.729>
69. Kim YS, Roesset JM (2004) Effect of nonlinear soil behavior on inelastic seismic response of a structure. *Int J Geomech* 4(2):104–114
70. Fatahi B, Tabatabaiefar SHR (2014) Fully nonlinear versus equivalent linear computation method for seismic analysis of midrise buildings on soft soils. *Int J Geomech* 14(4):04014016. [https://doi.org/10.1061/\(asce\)gm.1943-5622.0000354](https://doi.org/10.1061/(asce)gm.1943-5622.0000354)
71. Kamal M, Inel M, Cayci BT (2022) Seismic behavior of mid-rise reinforced concrete adjacent buildings considering soil-structure interaction. *J Build Eng* 51:104296
72. American Society of Civil Engineers (2017) Seismic evaluation and retrofit of existing buildings. American Society of Civil Engineer
73. Chopra AK (1995) *Dynamics of structures: theory and applications to earthquake engineering*, Pearson
74. Pacific Earthquake Engineering Research Center (PEER) (2015) NGA-East: Median ground-motion models for the Central and Eastern North America region. PEER Report No. 2014/05
75. Seissoft, Seismomatch software (2016) A Computer Program for Spectrum Matching of Earthquake Records. <http://www.seissoft.com>
76. Bolt BA (1973) Duration of strong ground motions. In: *Fifth World Conference on Earthquake Engineering*, vol 1, pp 1304–1313
77. El Hoseny M, Ma J, Josephine M (2022) Effect of embedded basement stories on seismic response of low-rise building frames considering SSI via small shaking table tests. *Sustainability* 14(3):1275
78. Wani FM, Vemuri J, Rajaram C (2022) Effect of soil structure interaction on the dynamic response of reinforced concrete structures. *Natural Hazards Research* 2(4):304–315
79. Standards Australia (2007) *Structural design action—Earthquake actions in Australia, AS1170.4*, Sydney, Australia
80. Akhtarpour A, Mortezaee M (2019) Dynamic response of a tall building next to deep excavation considering soil structure interaction. *Asian J Civil Eng* 20(4):479–502
81. Yeganeh N, Bazaz JB, Akhtarpour A (2015) Seismic analysis of the soil-structure interaction for a high-rise building adjacent to deep excavation. *Soil Dyn Earthq Eng* 79:149–170

Springer Nature or its licensor (e.g. a society or other partner) holds exclusive rights to this article under a publishing agreement with the author(s) or other rightsholder(s); author self-archiving of the accepted manuscript version of this article is solely governed by the terms of such publishing agreement and applicable law.